

COMPACTION PHYSICS OF SOLID ADDITIVE BLENDS
A THERMAL PROPERTIES STUDY

by

AMY BROWN

Presented to the Faculty of the Graduate School of
The University of Texas at Arlington in Partial Fulfillment
of the Requirements
for the Degree of

MASTERS OF SCIENCE IN MATERIALS SCIENCE AND ENGINEERING

THE UNIVERSITY OF TEXAS AT ARLINGTON

December 2013

Copyright © by Amy Brown 2013

All Rights Reserved

Acknowledgements

It is with the deepest gratitude that I thank my research advisor, Dr. Meletis, for his constant support and advice throughout my research.

I would like to thank my colleagues who supported me throughout my research process, especially Elad Har-Even. I am grateful to Elad for taking the time to help me prepare samples, provided me guidance, and offer a helping hand throughout my experiments. I would like to thank the rest of my research group who always provided supportive encouragement.

I cannot find the words to express my gratitude to my parents who provided me with the opportunity to pursue my graduate degree and who provided me with an extensive amount of support throughout my years at school. I would like to thank my boyfriend and friends who provided me with constant support, encouragement, and had patience with me as I finished my last semester of graduate school.

November 19, 2013

Abstract

COMPACTION PHYSICS OF SOLID ADDITIVE BLENDS
A THERMAL PROPERTIES STUDY

Amy Brown, M.S.

The University of Texas at Arlington, 2013

Supervising Professor: Efstathios I. Meletis

Committee Members: Harry F. Tibbals and Fuqiang Liu

Compacted solid additive blends have attracted the interest of the polymers industry due to their ability to improve processability. However, limited research has been performed to analyze the thermal properties that these additives have during pelletization.

This research studies the reaction behavior of erucamide and silica, when in a pure and mixed form, with each other when thermal conductivity and frictional heating experiments are conducted. During the thermal conductivity study, it was found that pure erucamide had a thermal conductivity of 0.37 W/mK. The thermal conductivity of pure silica could not be found since silica will not compact to itself. Therefore, the thermal conductivity was extrapolated and found to be 0.09 W/mK. With the higher thermal conductivity belonging to erucamide, the heat transference that occurs during pelletization is through the use of erucamide. During the frictional studies, it was found that erucamide had a lower coefficient of friction compared to silica. The samples used were not pure, meaning a presence of both silica and erucamide were present for all experiments. The value obtained for the sample with a 75wt% of erucamide was 0.26. The value obtained for the sample with 75wt% of silica was 0.53.

The surface and cross-section morphology and composition of the samples was examined by Scanning Electron Microscopy and Energy Dispersive X-Ray Spectroscopy. Through this a softened layer was seen that provided evidence of an outer protective layer that forms during the pelletization process. Further analysis into this formed softened layer for varying compositions provided critical temperatures that need to be reached during processing.

Table of Contents

Acknowledgements	iii
Abstract.....	iv
List of Illustrations	viii
List of Tables.....	xii
Chapter 1 Introduction and Motivation	1
1.1 Research Objective	2
Chapter 2 Process Description.....	4
2.1 Non-Melters	4
2.2 Binders.....	5
2.3 Compaction Process for Producing Solid Additive Blends	6
2.4 Post-Treatment	8
Chapter 3 Analysis Formulation	10
3.1 Thermal Properties	10
3.1.1 Effective Thermal Conductivity	11
3.1.2 Frictional Heating.....	13
Chapter 4 Experimental	18
4.1 Sample Preparation	18
4.2 Testing.....	23
4.2.1 Thermal Conductivity.....	23
4.2.2 Frictional Heating.....	25
4.3 Characterization.....	29
4.3.1 CRC-100 Sputtering	29
4.3.2 Scanning Electron Microscopy (SEM) and Energy Dispersive Spectroscopy (EDS)	29

Chapter 5 Results & Discussion.....	30
5.1 Compaction.....	30
5.1.1 Compaction Results.....	30
5.2 Thermal Conductivity	36
5.2.1 Thermal Conductivity Results	36
5.2.2 Scanning Electron Microscope Results	38
5.2.3 Energy-Dispersive Spectroscopy.....	40
5.3 Frictional Heating.....	45
5.3.1 Tribometer Testing.....	45
5.3.1.1 25% Erucamide- 75% Silica (Sample 1).....	46
5.3.1.2 50% Erucamide- 50% Silica (Sample 2).....	54
5.3.1.3 75% Erucamide-25% Silica (Sample 3).....	61
5.3.1.4 Total Frictional Work (\dot{W}_{TF}).....	68
5.4 Discussion	72
Chapter 6 Conclusion.....	79
Appendix A Determination of Critical Temperature	80
References.....	82
Biographical Information	84

List of Illustrations

Figure 2-1: A long chain fatty acid amide known as erucamide.(3).....	5
Figure 2-2: The cross-section of a pellet mill which shows the addition of raw material into the die and the compression and expulsion of a finished compacted pellet (6).	6
Figure 2-3: The pelletizing components that form a solid compacted pellet (6).	7
Figure 2-4: The bonding mechanisms that occur between the particles as compression proceeds (7).....	8
Figure 3-1: The set-up for measuring thermal conductivity of an unknown sample according to ASTM E1225-09 (9).....	12
Figure 3-2: The decrease in the coefficient of friction as more time passes allowing for the rearrangement of the slip additive (13).....	16
Figure 4-1: As-received form of a) erucamide and b) silica.....	19
Figure 4-2: The appearance of a) erucamide and b) silica after being crushed by the pestle.	20
Figure 4-3: The hardened steel chamber used to hold the material during the compaction process.	21
Figure 4-4: The Norco 12-ton hydraulic bottle jack used to compact the samples needed for experimentation.	22
Figure 4-5: The experimental set-up for finding the effective thermal conductivity.....	24
Figure 4-6: The sample holder for sample during tribometer testing.	27
Figure 4-7: The top view and side view of the CSM Tribometer that is used during the frictional heating experiments.....	28
Figure 5-1: The fully compacted samples after being expelled from the hardened steel chamber; with a) sample 1, b) sample 2, c) sample 3, and d) sample 4.	31
Figure 5-2: The bonding mechanisms that are present in sample 1.....	33

Figure 5-3: The bonding mechanisms that are present in sample 2.....	34
Figure 5-4: The bonding mechanisms that are present inside sample 3.	35
Figure 5-5: The change in thermal conductivity as the amount of erucamide increases.	37
Figure 5-6: The effective thermal conductivity change as temperature increases.....	38
Figure 5-7: The SEM micrographs of a) sample 4, b) sample 3, c) sample 2, and d) sample 1.	39
Figure 5-8: The penetration depth vs. wt % of erucamide that was measured.....	40
Figure 5-9: The original micrograph and elemental mapping for sample 1.	41
Figure 5-10: The original micrograph and elemental mapping for sample 2.	42
Figure 5-11: The original micrograph and elemental mapping for sample 3.	43
Figure 5-12: The original micrograph and elemental mapping for sample 4	44
Figure 5-13: The SEM micrograph showing the formation of a softened area at a 8mm radius.	47
Figure 5-14: The diameter of the wear track made by the pin.....	47
Figure 5-15: The SEM micrograph showing the formation of a softened area at a 11mm radius.	48
Figure 5-16: The diameter of the wear track made by the pin.....	48
Figure 5-17: The SEM micrograph showing the formation of a softened area at a 19mm radius.	49
Figure 5-18: The diameter of the wear track made by the pin.....	49
Figure 5-19: The measured coefficient of friction for the 8mm radius.	50
Figure 5-20: The measured coefficient of friction for the 11mm radius.	51
Figure 5-21: The measured coefficient of friction for the 19mm radius.	51
Figure 5-22: The relationship between temperature and depth for 8mm radius.	52
Figure 5-23: The relationship between temperature and depth for 11mm radius.	53

Figure 5-24: The relationship between temperature and depth for 19mm radius.	53
Figure 5-25: The SEM micrograph showing the formation of a softened area at a 10mm radius.	54
Figure 5-26: The diameter of the wear track made by the pin.	55
Figure 5-27: The SEM micrograph showing the formation of a softened area at a 15mm radius.	55
Figure 5-28: The diameter of the wear track made by the pin.	56
Figure 5-29: The SEM micrograph showing the formation of a softened area at a 20mm radius.	56
Figure 5-30: The diameter of the wear track made by the pin.	57
Figure 5-31: The coefficient of friction for the 10mm radius.	58
Figure 5-32: The coefficient of friction for the 15mm radius.	58
Figure 5-33: The coefficient of friction for the 20mm radius.	59
Figure 5-34: The relationship between temperature and depth for 10mm radius.	60
Figure 5-35: The relationship between temperature and depth for 15mm radius.	60
Figure 5-36: The relationship between temperature and depth for 20mm radius.	61
Figure 5-37: The SEM micrograph showing the formation of a softened area at a 15mm radius.	62
Figure 5-38: The diameter of the wear track made by the pin.	62
Figure 5-39: The SEM micrograph showing the formation of a softened area at a 17mm radius.	63
Figure 5-40: The diameter of the wear track made by the pin.	63
Figure 5-41: The SEM micrograph showing the formation of a softened area at a 20mm radius.	64
Figure 5-42: The diameter of the wear track made by the pin.	64

Figure 5-43: The coefficient of friction for the 15mm radius.	65
Figure 5-44: The coefficient of friction for the 17mm radius.	66
Figure 5-45: The coefficient of friction for the 20mm radius.	66
Figure 5-46: The relationship between temperature and depth for 15mm radius.	67
Figure 5-47: The relationship between temperature and depth for 17mm radius.	68
Figure 5-48: The relationship between temperature and depth for 20mm radius.	68
Figure 5-49: The relationship between total frictional work and depth for sample 1.	71
Figure 5-50: The relationship between total frictional work and depth for sample 2.	71
Figure 5-51: The relationship between total frictional work and depth for sample 3.	72
Figure 5-52: How the melted shell forms from the heat transfer that occurs inside the press channel (1).	73
Figure 5-53: The relationship between thermal conductivity and penetration depth.	74
Figure 5-54: The relationship between temperature and depth for sample 1.	75
Figure 5-55: The relationship between temperature and depth for sample 2.	75
Figure 5-56: The relationship between temperature and depth for sample 3.	76
Figure 5-57: The change in frictional work as the wt% of erucamide increases.	77
Figure 5-58: The relationship between normalized total frictional work with thermal conductivity and critical depth.	78

List of Tables

Table 4-1: Table of compositions for the model system of erucamide and silica.	18
Table 4-2: The sample compositions of erucamide and silica.	20
Table 5-1: The densities of the discs that were compacted for the thermal conductivity experiments.	30
Table 5-2: The measured effective thermal conductivity obtained experimentally.	36
Table 5-3: The measured penetration depth that evolved through the effective thermal conductivity experiments.	40
Table 5-4: The elemental weight percent of silicon, carbon, and oxygen in sample 1.	41
Table 5-5: The elemental weight percent of silicon, carbon, and oxygen in sample 2.	43
Table 5-6: The elemental weight percent of silicon, carbon, and oxygen in sample 3.	44
Table 5-7: The elemental weight percent of silicon, carbon, and oxygen in sample 4.	45
Table 5-8: The different experiments that were conducted using the tribometer.	46
Table 5-9: The total frictional work each sample experienced.	70

Chapter 1

Introduction and Motivation

The pelletization of raw materials has been a process which has been used for over one hundred years with a large focus on biomass or wood pellets. The first patent for a pelletization process describes sawdust being heated to 150°C and then placed into a strong mold where it was then compressed using a steam hammer (1). The key factors that affect the pelletizing process have been under investigation over the last couple of years. In the case of compacting wood pellets, it has been found that the main process parameters that affect the product are moisture content, temperature, particle size, press channel dimensions, and pelletizing pressure (1). The compaction of wood pellets and understanding the process parameters shows that compacting and pelletizing raw materials together is a promising field that can help other industries.

The compaction of additive blends is a new venture in the polymers industry which can provide promising improvements in the processability of the industrial practice of additives. For years the industry has been working with powders as the main form for additive delivery during the extrusion of polymers. This process is long, tedious, and can cause many problems for the companies as well as the workers (2). However, with the increased use of the compacted additive blends, manufactures are developing steps within the process to mitigate many of the problems associated with using powder additives.

An important objective for the compacted additive blends is to increase process efficiency, reduce overall manufacturing costs, and reduce health and environmental risks over use powder additives (2). Some specific advantages for producing and supplying compacted blends over using powder additives are:

- Compacted blends will come in a prepackaged form enhancing transportation, pellet handling, and can be premeasured for efficient introduction to a fabrication process.
- Compacted blends minimize particulate matter reducing exposure to workers and providing a more sanitary work environment.
- Compacted blends provide the opportunity for variable blends to be made yielding opportunities in the engineering process for cost comparisons or mechanical property trades.

1.1 Research Objective

Pelletizing process is a combination of different factors acting on raw materials in order to produce a stable solid compacted pellet. The different factors that occur include compression, flow, and friction. During compression, the raw material is crushed by a mechanism and the distance between each particle is reduced. Mechanical bonding begins to occur in the form of solid bridges and/or molecular forces. As material is pushed into the press channel by the mechanism a flow component is introduced. During the flow process, more and more raw material is pushed into the press channel causing thin layers to stack up onto each other. The force that is acting on the material to push it further into the press channel induces friction due to the raw material sliding against the press channel wall. Friction creates heat resulting in a temperature rise and micro-melting along the surface of the compacted material takes place.

In order to understand what takes place inside the press channel as the material is being formed into a stable pellet, several experiments will be conducted with the objective to isolate this frictional process. The frictional heat components is comprised of thermal conductivity into the die and thermal conductivity into the pellet that help bond and form the final stable pellet.

Determination of the thermal conductivity of the raw materials in the pellet is important in order to help explain how well heat can be transferred into the pellet. Thermal conductivity of the pellet will also help determine how the outer shell of the pellet is formed.

The specific objective of this to study is to determine the frictional heat generation during the compaction process and the effective thermal conductivity of compacted pure and mixed powders to characterize the shell created during the compaction process. Knowing the conditions the produce the shell will facilitate determination of a stable pellet to support transportation, handling, and use in manufacturing environments.

Chapter 2

Process Description

The process to produce solid additive blends can be summarized in 3 steps: pre-treatment, pelletization, and post-treatment (1).

During the pre-treatment phase, the initial materials that will be forming the pellet are selected. The desired materials must fit into certain characteristics or material requirements that a customer may specify for the solid additive blends. Regardless of material requirements, these solid additive blends must have at least one additive that is a “non-melter” and another additive that is a “binder”. The raw material will then go through a conditioning process which could include size reduction and mixing to form a homogenous powder mixture in order to be deemed ready for the pelletization process.

2.1 Non-Melters

In the polymers industry, it is important when making compacted additive blends to have an additive that has a high melting temperature of at least 300°C or greater, typically called a non-melter. A non-melter is an important part of the additive blend because it does not melt while passing through the press channel and provides desirable properties to the final product. It helps with keeping the blend solid since its melting point is higher than the temperature rise due to heat that is generated from friction. If a non-melter is not selected the pellet would not form. Instead, a paste like substance would form and stick to the press channel walls and die causing the machine to no longer work properly. There are several non-melters that are commonly used throughout the polymers industry such as silica, phenolic antioxidant, and phosphite antioxidant.

Silica is a natural mineral, but when produced synthetically it consists of amorphous silicon dioxide. Synthetic silica (SiO_2) is used as an anti-blocking additive (3). In the polymers industry, blocking is a major problem which occurs under strong Van der

Waals forces between the amorphous regions of the polymer. During compaction, as the distance between the two layers is reduced the forces increase causing an increase in the blocking behavior (4). An anti-block additive is used to reduce the occurrence of the Van der Waals forces. The additive creates asperities between the two layers which minimizes the contact between the layers, increases the distance, and minimizes the blocking (4).

2.2 Binders

In the polymers industry, it is important when making compacted additive blends to have an additive that has a low melting temperature around or below 100°C, typically called a binder. A binder is an important part of the additive blend because it softens while being pushed down the press channel due to the frictional heat generation. With softening, the binder is able to combine and flow into the non-melter and form a solid compacted pellet. There are several binders that are commonly used throughout the polymers industry, the most common being erucamide.

Erucamide comes from a mono-unsaturated C22 erucic acid and is part of the fatty acid amide group (3). Erucamide is used as a slip additive in many processing techniques because such additives provide an internal lubricant that reduces friction and improves slip. Some of the advantages of using erucamide are that it has a lower volatility, good heat stability, better blocking performance, and a lower final coefficient of friction (5). The chain of erucamide is depicted in Figure 2-1:

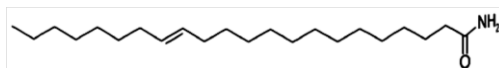


Figure 2-1: A long chain fatty acid amide known as erucamide.(3).

2.3 Compaction Process for Producing Solid Additive Blends

During the pelletization phase, the homogenous powder mixture is fed into a pellet mill that consists of a die, rollers, and a press channel with each part serving an instrumental role in the process. A cross-section of a pellet mill is illustrated in Figure 2-2.

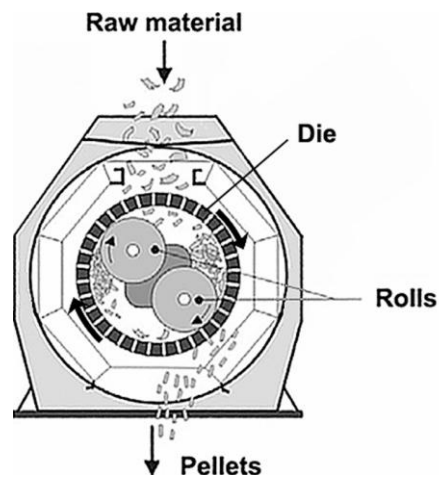


Figure 2-2: The cross-section of a pellet mill which shows the addition of raw material into the die and the compression and expulsion of a finished compacted pellet (6).

The pelletizing process is a continuous process in which raw materials (e.g. powders) are continuously being added into a die by means of the feedstock (6). The die works alongside the rollers in order to pass the raw material down into its interior. The die's interior consists of numerous perforated closely spaced channels as well as bearing-mounted stationary rollers which are utilized when the die is in a continuous circular motion. As powder is being continuously feed into the pellet mill, the die is moving in a circular motion allowing the rollers to compress and bond the incoming powders together. The powder is then pushed into several press channels along the die. Each time the rollers passes by a press channel, a new layer of powder is pushed into

the press channel. Causing a downward motion to the rest of the powder that is already inside the press channel and creating a cylindrical pellet with a known diameter. Further detail of the compaction process is shown in Figure 2-3 (6). In this detail, the macro process can be considered in the micro level as three distinct components which are compression, flow, and friction which are highlighted in Figure 2-3 (6).

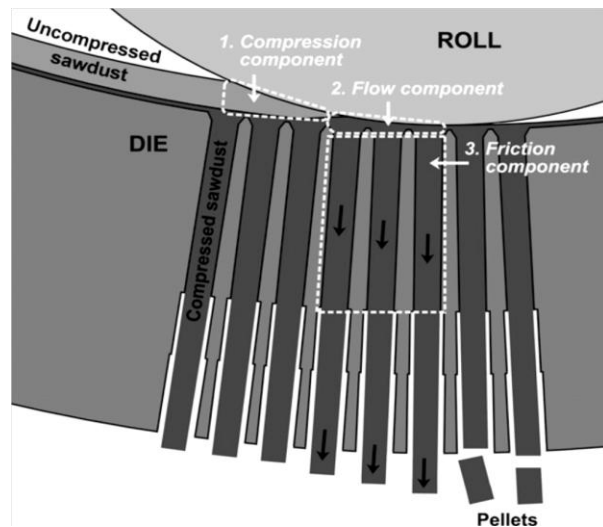


Figure 2-3: The pelletizing components that form a solid compacted pellet (6).

During compression, the die begins to move allowing the roller to compress the powder together. The powder begins to create tight contact with its surroundings, any remaining air pockets have escaped, and a certain density is reached that is similar to the final pellet density. This tight contact can be attributed to solid bridges, mechanical interlocking, or inter-particle bonding which all play a role in holding the final solid compacted pellet together as shown in Figure 2-4.

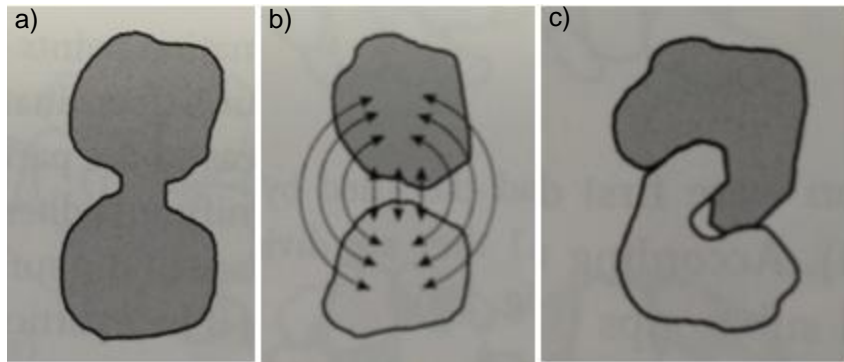


Figure 2-4: The bonding mechanisms that occur between the particles as compression proceeds (7).

As the roller passes over the compressed powder, it begins to push the powder into the press channels leading to the next step in the compaction process which is flow. As more powder is added into the press channel, it combines with the powder that was previously inside the press channel. The distance between the two layers is reduced dramatically and the continuous solid mass reaches its final density. As the roller continues to force more powder inside the channel, the compacted mass begins to move farther into the channel. As the compacted cylindrical mass slides down into the channel, a frictional force is generated. The third and final component to compaction is now reached. The pressure from the roller, however, is strong enough to overcome this frictional force and the compacted cylindrical mass is able to exit the press channel.

2.4 Post-Treatment

The post-treatment of the pellets occurs right after a pellet has been ejected from the press channel on the pellet mill. When the pellets are first pushed out of the press channel, their temperature is quite high due to two separate interactions. The first interaction occurs when the pellet is stationary inside the press channel for a certain amount of time. The second interaction is due to the frictional heat that arises from the

contact between the press channel wall and the powder/pellet shell. The pellets are moved to a pellet cooler where the pellets are able to be cooled back to room temperature. After some time, they are then screened to eliminate small particles.

As illustrated, the making of a stable compacted cylindrical pellet which maintains shape, size, and density is a tedious process that requires great knowledge of several factors. Of the many factors contributing to the formation of a pellet, two critical properties that are the focus of additional investigation are the frictional heating properties and thermal conductivity properties. Frictional heating is represented by the movement of two objects sliding past one another thus, causing a frictional force which in turn causes heat and a temperature rise to occur. The thermal conductivity will represent how well a certain amount of heat is able to penetrate into the compacted cylindrical pellet while inside the press channel. These properties represent how the pellet is able to maintain its shape once exiting the press channel and will help develop an understanding about the pelletization process.

Chapter 3

Analysis Formulation

3.1 Thermal Properties

Thermal properties play a major role during the production of a stable solid compacted pellet. It is known that during the pelletization process, heat is generated inside the press channel due to friction being produced between the walls of the press channel and the raw materials being forced inside the press channel. Stelte highlights that during biomass pellet production, the temperature of the die under normal operation is around 90°C and the temperature of the pellet leaving the press channel is around 70°C (1). The temperature difference between the die and the produced pellet is somewhat considerable due to the inability of the metal surface to transfer heat into the pellet and the short time that the pellet is inside the press channel. The limited heat transfer that penetrates into the pellet helps it form a shell and produce a stable pellet.

As previously discussed, the two components needed to produce a solid additive blend are a non-melter and a binder. Stelte highlights that in order to produce a more stable pellet, thin layers of waxes, as the binder, are needed. The waxes melt during the pelletization process, serve as adhesive between the different biomasses, and then solidify quickly after pelletization is complete (1).

Increasing temperature has shown that the stabilization of pellets has increased; reduced the friction in the press channel due to improved additive blend mechanical properties, and lower energy requirements for the different components used during the pelletization process (1). Thermal properties play such a large role in the production of a stable solid compacted pellet, it is important to understand how they affect the overall end product.

3.1.1 Effective Thermal Conductivity

Thermal conductivity is a measure of how well a material is able to conduct heat intrinsically throughout its surroundings. In the presence of a temperature gradient, heat transfer will take place within the material. Heat transfer will take place in the direction of decreasing temperature. When a higher temperature is present, a greater amount of molecular energy is also present. According to thermodynamics, a shift will occur from the higher energy state to a lower energy state, thus, causing conduction of heat to flow to the lower energy state.

Calculating the effective thermal conductivity was performed experimentally following a setup used by Hadley. This experimental setup provides for a favorable utilization of the steady-state condition because the temperature is set and does not change with time. Hadley explains that when maintaining a temperature gradient, a steady-state heat flow is introduced in the stack of cylindrical discs (8). For the top and bottom discs to be useful references, they are made-up of the same material. This allows for both discs to have an identical heat flux and therefore, the thermal conductivity will be known. The temperature differences that are present in the reference discs due to the temperature gradient and the known thermal conductivity of the reference discs are used to determine the thermal conductivity of the unknown sample (8).

Thermal conductivity test measurement setup followed Hadley's method, but disc stacks and equipment setup closely aligned with the comparative method utilized for the determination of the effective thermal conductivity for unknown samples in ASTM standard E1225-09 shown in Figure 3-1.

$$q'_B = \lambda_M \times \frac{T_6 - T_5}{Z_6 - Z_5} \text{ (Bottom Reference Disc)} \quad (2)$$

where q'_T and q'_B are the heat flow per unit area (W/m^2) into the top and bottom reference bar, respectively; λ_M is the thermal conductivity (W/mK) of the meter bars; T is the absolute temperature (K) measured by each thermocouple; and Z is the position as measured from the upper end of the column (m) (9). The determination of the sample's thermal conductivity, λ'_S , can then be found by using

$$\lambda'_S = \frac{(q'_T + q'_B)(Z_5 - Z_2)}{2(T_5 - T_2)} \quad (3)$$

where Z is the length of the sample including some reference material and T is the absolute temperature over the range of the sample (9). The sample that was utilized during this experimentation was a compacted powder; therefore, thermocouples were not directly inserted into the specimen but had thermocouples placed into the reference bars close to the interface. In order to verify that the measured effective thermal conductivity of the sample is accurate, a cylindrical standard sample was placed in-between the two cylindrical reference discs and the effective thermal conductivity of the standard sample was measured (10).

3.1.2 Frictional Heating

Friction is a process that arises when two objects are slid past one another under load. During the compaction process, as the compacted powder mixture slides down the press channel against the walls friction develops. There are a few key events that occur due to this frictional process; one is a rise in temperature along the interface between the channel wall and the powder mixture and second is the need for higher pressure to push the mixture down into the press channel in order to overcome the friction that is being created. The scope of this study considers only the temperature rise that occurs inside the press channel along the interface.

Frictional heating is very important because during compaction the homogenous powder mixture begins a “melt” process due to the interface interaction occurring between the press channel wall and the powder. As the press channel wall-powder interaction occurs energy in the form of work is produced from the frictional force, F , that is developed along die channel distance, x (11).

The product from friction force, F , and sliding velocity, v , explains the rate at which energy is put into the system (11). The energy input rate is balanced by heat conduction because heat will either be dissipated into the contacting solid or the surroundings (11). The more energy that is produced due to the increase in the friction force the higher the temperature at the interface between the die channel and powder will be.

As this interface interaction is occurring between the compacted powder and the press channel wall, a mean surface temperature is reached throughout the interface. This mean surface temperature decreases from the edge to the center of the bulk material. The amount of variation from the edge to the center will depend on the thermal conductivity of the bulk material. If the surface temperature that is reached at the interface is high enough the softening process will begin. As the pellet continues down the channel and starts to exit the die, heating of the contact surface will stop. Once heating has stopped, it will diffuse into the pellet structure cooling at the contact surface and forming the outer shell which helps form the pellet structure.

Another phenomenon from friction is flash temperature. A flash temperature will occur at individual interaction points, asperities, between the powder and the press channel wall. This means that at different interaction points, there could be varying flash temperatures. This will induce a change in the blend’s morphology because the “binder” part of the blend will begin to experience a rise in surface temperature due to the

interface that has been produced (12). The “binder” will then undergo a local melt or softening process due to the frictional heat that is generated.

As the “binder” undergoes this softening or melt process, there is an impact on the coefficient of friction. The “binder” can be engineered to be a lubricant. Many binder “lubricants” are fatty acid amides. When the “binder” and “non-melter” are mixed together, there is a difference in surface energies which causes the “binder” to migrate towards the surface. As the “binder” migration to the surface occurs, a rearrangement process begins. Since fatty acid amide groups are composed of a hydrocarbon chain and an amide group. The hydrocarbon chain will be embedded into the “non-melter” (polymer) while the amide group orient to the surface. As more “binder” migrates to the surface, the rearrangement continues with the amide-amide group facing each other and the hydrocarbon chain facing the surface. This process continues until the amount of “binder” migrating to the surface is close to zero resulting in decrease in the coefficient of friction is seen similar to Figure 3-2 (13).

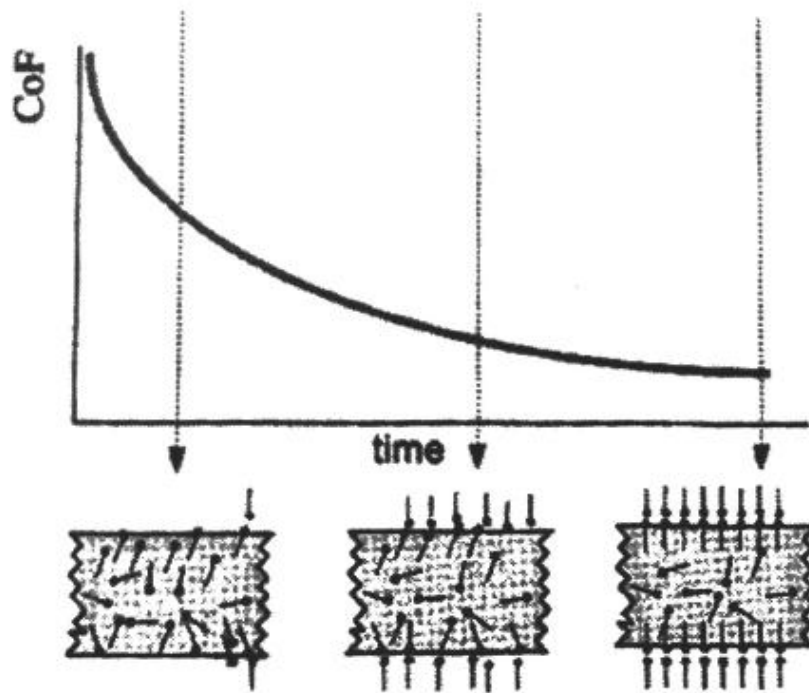


Figure 3-2: The decrease in the coefficient of friction as more time passes allowing for the rearrangement of the slip additive (13).

The coefficient of friction describes the ratio of the force to slide one object over the other and the force that is pressing them together. During the compaction process, a frictional force is produced between the press channel wall and the compacted powder mixture while another force, from the roller, is pressing more powder into the press channel. In the beginning of compaction, the coefficient of friction is high because the amount of force needed to overcome static friction is high. However, as compaction continues, the press channel temperature will begin to increase due to the friction. This will cause the “binder” to soften allowing for easier movement down the press channel and thus, reducing the coefficient of friction to a lubricated friction value. The frictional work, \dot{W}_f , can then be found using

$$\dot{W}_f = P \times u \times \mu \quad (4)$$

where μ is the coefficient of friction, P is the applied pressure, and u is the sliding velocity (m/sec) (14). Therefore, it is seen that frictional heating has a major impact on the final shape of the compacted powder as well as the properties that are exhibited by the components (15).

Chapter 4

Experimental

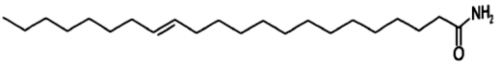
4.1 Sample Preparation

In order to perform the experiments to determine the thermal conductivity and frictional aspects of the pellet, a model system was selected. Considerations used in production of the model system included:

- 1) The system must contain a “binder” component which has a lower melting point and a “non-melter” component which has a higher melting point.
- 2) The system must be representative of additive blends applicable to the polypropylene/polyethylene resins that are used in the polymers industry.

To meet these considerations, my model system was constructed out of erucamide and silica which are both common to the industry. Table 4-1 presents the model system of erucamide and silica along with different sample compositions that were used during the experiments to provide a full picture into how each component reacts during the compaction process.

Table 4-1: Table of compositions for the model system of erucamide and silica.

Components	Chemical Formula	Additive Function	Melting Temperature (°C)
Erucamide		Slip Additive/Lubricant	83.0
Silica	SiO ₂	Anti-Blocking	> 300

Sample:	Sample Composition:
1	25% Erucamide- 75% Silica
2	50% Erucamide- 50% Silica
3	75% Erucamide- 25% Silica
4	100 % Erucamide

The physical appearance of erucamide and silica is very different from one another. Erucamide, known as Crodamide ERBead, comes in the shape of small beads with an opaque whitish color as seen in Figure 4-1a. Amorphous Silica, known as Gasil AB725, is a very porous powder that is very light and fluffy with a particle size of 4-5 μ m as seen in Figure 4-1b.

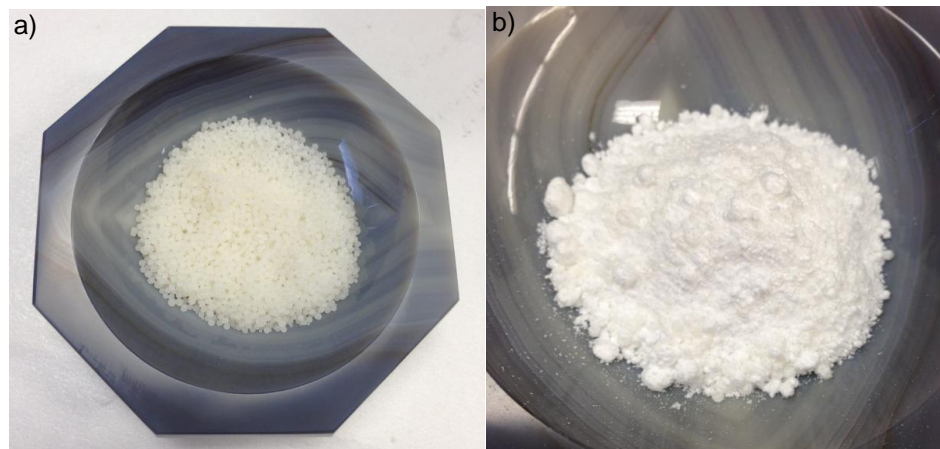


Figure 4-1: As-received form of a) erucamide and b) silica.



Figure 4-2: The appearance of a) erucamide and b) silica after being crushed by the pestle.

Before the compaction process, the appropriate amounts of erucamide and silica were mixed. Each pellet has a total weight of 10 grams. Each sample's composition is made up of varying amounts of erucamide and Table 4-2 shows the composition by weight of erucamide and silica.

Table 4-2: The sample compositions of erucamide and silica.

Sample	Weight of Erucamide (g):	Weight of Silica (g):
1	2.5	7.5
2	5.0	5.0
3	7.5	2.5
4	10.0	0.0

After weighing each sample, erucamide and silica were pulverized by a mortar and pestle to simulate the action that occurs inside of a pelletizing machine with Figure

4-2 showing the final product. After crushing, both materials were added together and mixed in order to make a homogenous powder mixture.

To simulate the process of making a compacted pellet, a simulated pelletizing machine was assembled. The simulation has many parts that together produce similar results to that of the press chamber and roller. To produce the press channel, a hardened steel cylinder, shown in Figure 4-3, was fabricated with a removable bottom. A piston that fits tightly inside the cylinder in order to compress the powder was also fabricated. A Norco 12-ton hydraulic bottle jack, shown in Figure 4-4, was used as the roller in order to apply pressure on to the powder for compaction. A pressure gauge was installed on the side of the hydraulic bottle jack to measure the pressure level change as compaction progressed. A caliper was used to measure the change in distance as the blend was compressed.

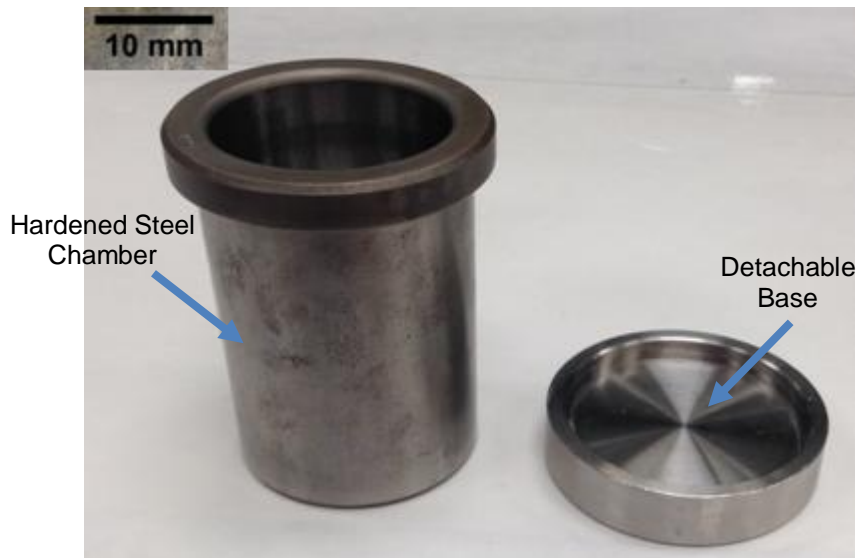


Figure 4-3: The hardened steel chamber used to hold the material during the compaction process.

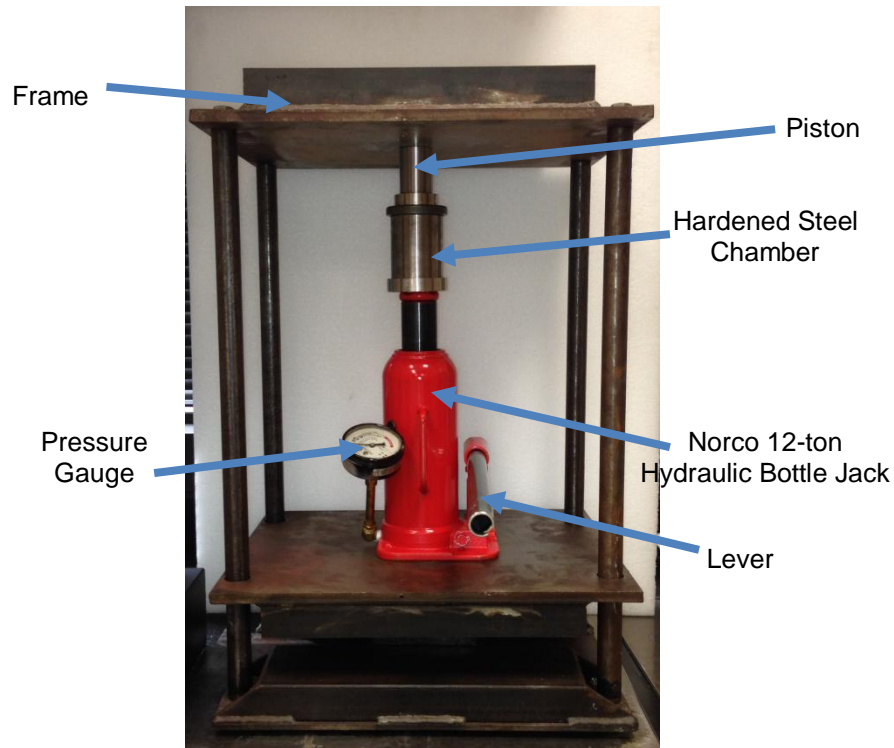


Figure 4-4: The Norco 12-ton hydraulic bottle jack used to compact the samples needed for experimentation.

Urethane mold release was sprayed on all the surfaces of the hardened steel chamber, the powder mixture was placed inside the chamber, and pressure was then applied. The pressure level for complete pelletization was not known. However, the density of the compacted pellets is known to be 0.85 to 1.05g/cm³. A calculation was made for the sample height to achieve this known density, ρ :

$$\rho = \frac{m}{D^2 \times H} \quad (5)$$

where m is the sample mass, D is the diameter of the die chamber, and H is the sample height. Once the desired height was obtained for the correct density, the pressure was released and the pellet was removed from the chamber. The final weight and height of

the newly compacted pellet were measured and the overall density was calculated to verify the pellet fell within the known range.

4.2 Testing

4.2.1 Thermal Conductivity

Studying the effective thermal conductivity of compacted powders is a key issue in the compaction process described above. During the compaction process, thermal properties are initiated inside the press channel by binder micro-melting causing the compacted powder to form a melted shell which helps form a pellet structure. According to Leung et al. many ASTM standard techniques were critiqued before using a comparative method which follows ASTM 1225-04 (10). The rule of mixtures was also utilized in the method in order to determine the unknown effective thermal conductivity of the powder mixture.

Thermal conductivity was experimentally measured using an adaptation of ASTM standard E1225-09 the “Standard Test Method for Thermal Conductivity of Solids by Guarded-Comparative-Longitudinal Heat Flow” using a custom-built laboratory system. The system is made up of two 304 stainless steel cylindrical discs that are 2” in diameter and are 1” thick. The 304 stainless steel was chosen because it has a known thermal conductivity and is able to measure conductivity of a sample between 0.037 to 113 $\text{Wm}^{-1}\text{K}^{-1}$ (8). Each 304 stainless steel disc has two holes drilled in halfway with each hole is about 1/16” in diameter.

The sample with an unknown thermal conductivity was produced of the following combinations set forth by Table 4-1 with the compaction parameters detailed above. The sample was then placed in-between the two reference discs coated with a non-silicone heat transfer compound on the sides that contact the sample. A heat source, also with a

2" diameter, was placed on top. The bottom reference disc was placed onto a heat sink that was used to reduce thermal contact resistance.

Thermocouples were placed into each reference disc to measure the temperature gradient that formed throughout the experiment. A stainless steel cylinder, with a 2" diameter, was used to apply pressure to provide good contact between all the surfaces. A fiberglass insulating material was placed around the column to prevent heat loss.

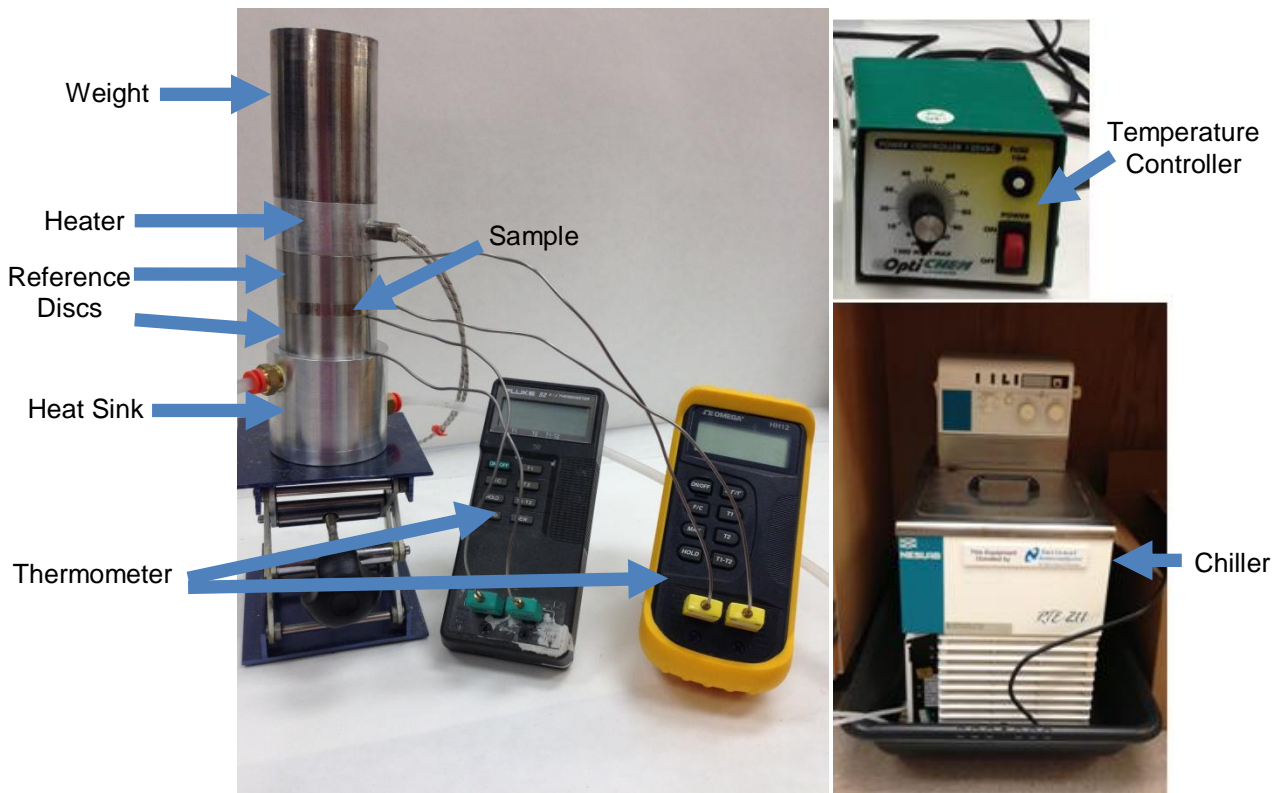


Figure 4-5: The experimental set-up for finding the effective thermal conductivity.

A baseline temperature measurement was obtained while the chiller was at 15°C and the temperature controller was at 0% to represent the beginning stages of the pelletization process.

After the temperatures were taken, the temperature controller was raised to 4%. When the temperature stabilized after the temperature rise, another reading was obtained. Each time steady state was reached, the temperature controller's power setting was increased by +4%. The power setting was continually increased until the temperature of the top reference disc was around 80 to 84 °C; typically reached at a power setting of 20%. The reference disc was at the melting point of erucamide; however, the contact temperature between the sample and the bottom of the top reference disc was around 51 °C. This temperature is when erucamide begins to soften and represents the temperature that the pelletizing machine reaches while producing pellets.

The two reference discs have an assumed identical heat flux. Following this assumption, the rule of mixtures was utilized to calculate the unknown effective thermal conductivity. The rule of mixtures states that the thermal conductivity of the sample depends on the properties of the reference discs. Equation 1 was rearranged to isolate thermal conductivity; k . Each reference disc's heat flow, Q , was calculated and the average was found. This average heat flow was used to find the sample's effective thermal conductivity by multiplying by the change in height over the change in temperature across the sample (8; 16).

4.2.2 Frictional Heating

Frictional heating inside the press channel influences the overall melting/softening of the "binder" in the compacted powder. Understanding this gives insight into how frictional heating affects the formation of the outer shell, and explains how much melting occurs inside the press channel in order to keep the newly formed pellet a stable/durable mass.

An experimental investigation was conducted into what frictional heating occurred between the powder and press channel walls during compaction. The friction coefficient is measured using a pin on disk tribometer called an CSM Instruments Tribometer. The frictional measurements were done on samples 1, 2, and 3 from Table 4-1. The frictional testing is performed using parameters that are typically seen in the industry. A load of 1-2 N is used for the test. The velocity that a compacted pellet experiences when being expelled from the press channel is between 70-200 mm/sec; therefore a sliding velocity at 100mm/sec, 10cm/sec, is a workable average that was used for all the experiments. A certain amount of laps assumed because it was important to know how many times each specific spot was touched during an experiment. The amount of laps and the change in load that each experiment was conducted at varied in order to determine how well heat was able to penetrate into the sample.

The pellet sample holder, shown in Figure 4-6, was manufactured out of stainless steel 304. Screws were added so the pellet sample would not slip during the tribological testing. The pellet sample was placed into the sample holder and was checked to make sure it was flush all around.

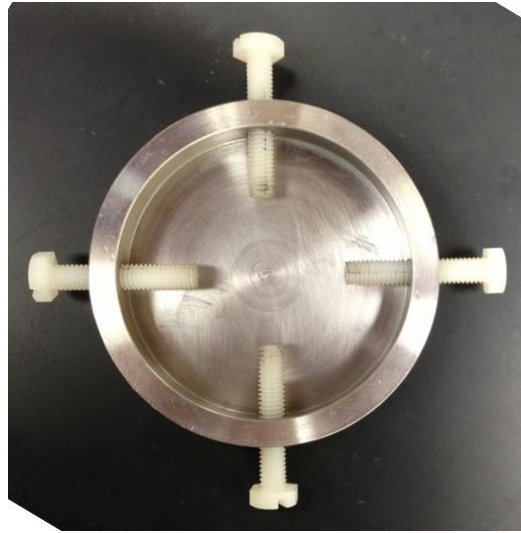


Figure 4-6: The sample holder for sample during tribometer testing.

The sample holder was then placed onto the tribometer's mandrel, shown in Figure 4-7, where it is tightened into place. Next the pin was adjusted in order to make it level on the sample. Careful manipulation of the counterweights was performed so pin will stay on the sample. The radius was then adjusted by turning the crank handle. Once all these parameters were adjusted accordingly, a load was added onto the top of the pin.

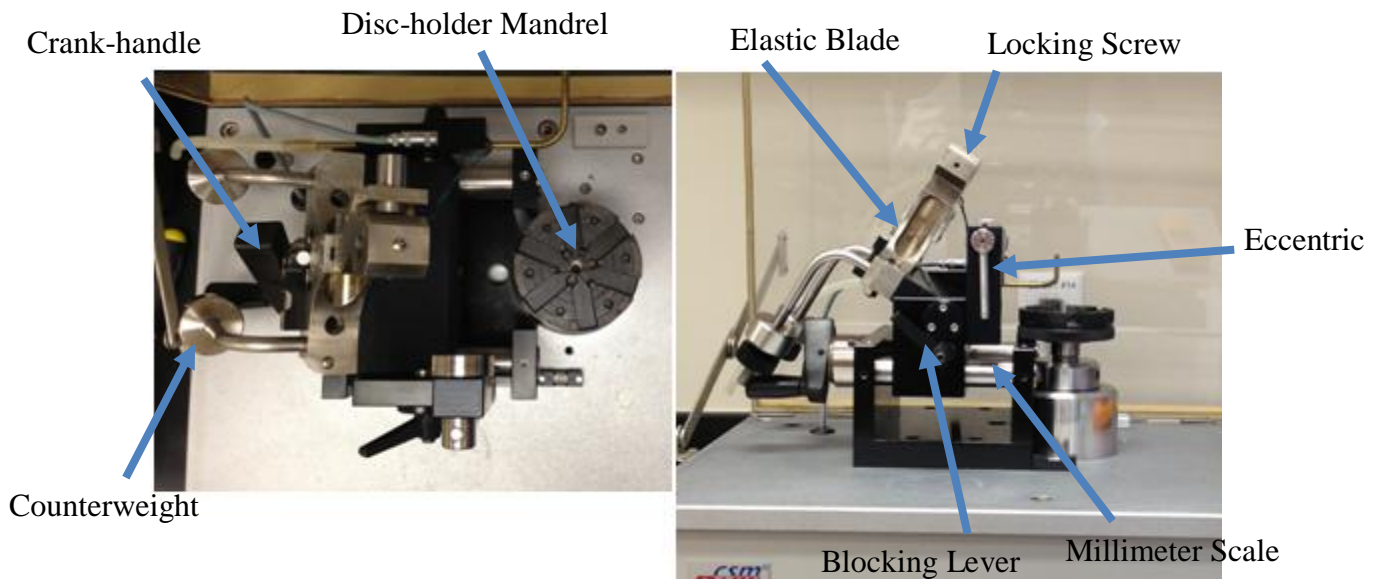


Figure 4-7: The top view and side view of the CSM Tribometer that is used during the frictional heating experiments.

Then using the software, TriboX 2.10.C, information concerning the sample was entered such as: humidity, acquisition rate, sample temperature, load, radius, number of laps, and linear speed.

With using the coefficient of friction that was obtained through the experiment, equation two is used to calculate the frictional work. Each experiment's graph displays a leveling off point for the coefficient of friction, therefore, this was the coefficient of friction used in the calculation. Pressure, P , was also calculated through the load that was used, F , and the area, A , of contact that the pin had with the sample.

$$P = \frac{F}{A} \quad (6)$$

The area was calculated using the diameter, D , found from each sample's wear track.

$$A = \frac{\pi}{4} \times D^2 \quad (7)$$

The area of contact varied with each test so it was adjusted accordingly in the calculation.

Equation 2 represents the work that occurs after the sample has come into contact with

the pin once. In order to determine the total frictional work, W_{Tf} , that the sample experiences, equation 7 is used

$$\dot{W} = L_T \times W_f \quad (8)$$

where L_T is the total amount of laps and, W_f , is the frictional work done by one lap. A relationship was then found between total frictional work and depth.

4.3 Characterization

4.3.1 CRC-100 Sputtering

A Plasma Sciences Inc. CRC-100 Sputtering System was used to coat the samples, from Table 4-1, in order to create a conductive layer. During sputtering, a carbon target was used with a four minute processing time at a processing pressure of 8millitorr and a current of 10mA. During The target used to sputter was carbon

4.3.2 Scanning Electron Microscopy (SEM) and Energy Dispersive Spectroscopy (EDS)

A Hitachi S-3000N variable pressure SEM was used along with an EDS attachment to study the surface and cross-section morphology as well as the chemical composition of the samples from Table 4-1. The low vacuum and high vacuum function of the SEM were both utilized at different magnifications. The acceleration voltage used during these processes ranged from 10kV to 20kV while the working distance varied between 12-20mm.

Chapter 5

Results & Discussion

5.1 Compaction

5.1.1 Compaction Results

The compaction experiments produced a compacted disc with the density typically seen in the industry. When a pressure around 5-6 bars was reached a fully compacted disc was produced. The densities of the compacted discs used for the thermal conductivity experiments are shown in Table 5-1.

Table 5-1: The densities of the discs that were compacted for the thermal conductivity experiments.

Sample:	Density (g/cm^3) of Thermal Conductivity Samples:	Density (g/cm^3) of Frictional Heating Samples:
1	0.63	0.55
2	0.78	0.79
3	0.85	0.94
4	0.85	-----

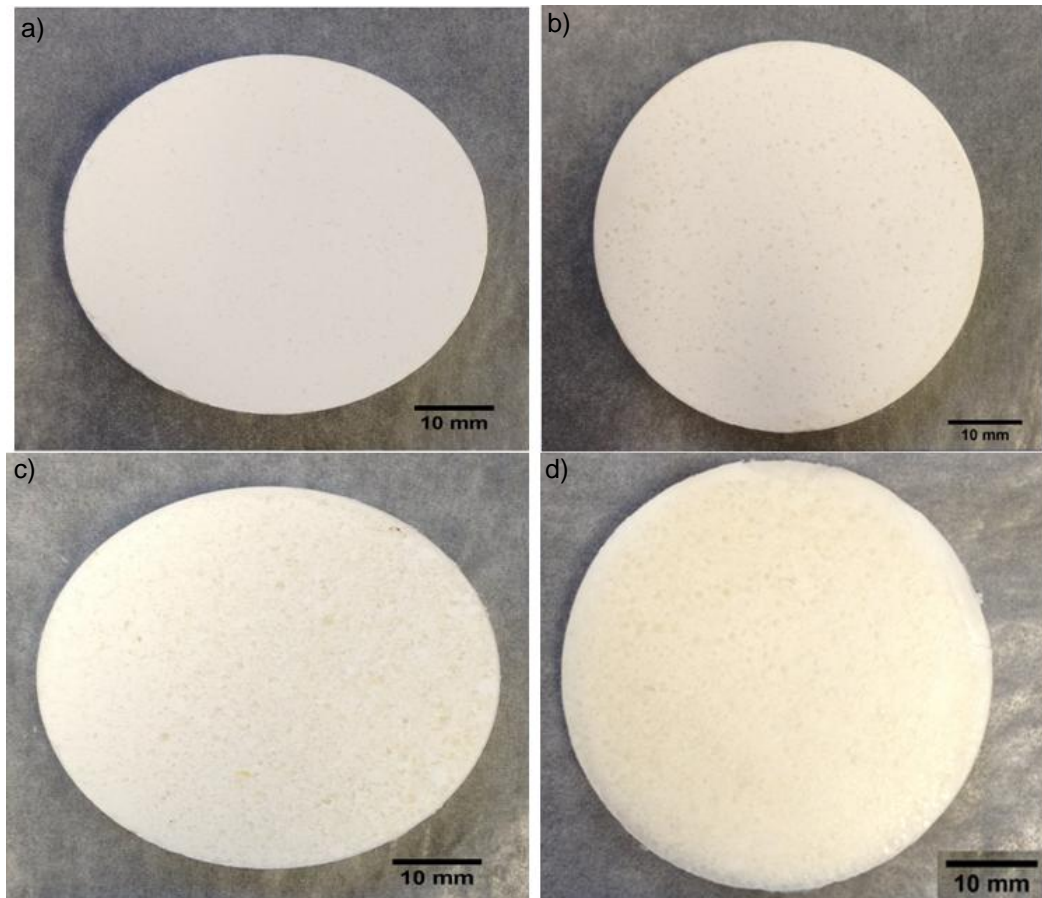


Figure 5-1: The fully compacted samples after being expelled from the hardened steel chamber; with a) sample 1, b) sample 2, c) sample 3, and d) sample 4.

Erucamide is known as a binder so the greater amounts of erucamide present the easier compaction will be. The bonding mechanisms were also affected when the amount of erucamide present decreased in each disc. This is due to silica not compacting easily because of its porous nature which causes more space in-between individual particles. Therefore, the more distance present in-between individual particles inside the compacted disc the smaller the amount of bonding mechanisms that will be present.

Therefore, the density that was achieved was reduced when the amount of erucamide in each mixture decreased.

The bonding mechanisms such as solid bridges, molecular forces, and mechanical interlocking play a large role during compaction. As pressure increased bonding between the individual particles takes hold to form the final compacted disc.

Figure 5-2, Figure 5-3, and Figure 5-4 show the bonding mechanisms that occur after compaction in samples 1, 2, and 3, respectively. All three bonding mechanisms are shown in the compacted sample with the red circle representing solid bridges, the blue circle representing mechanical interlocking, and the purple circle representing molecular forces.

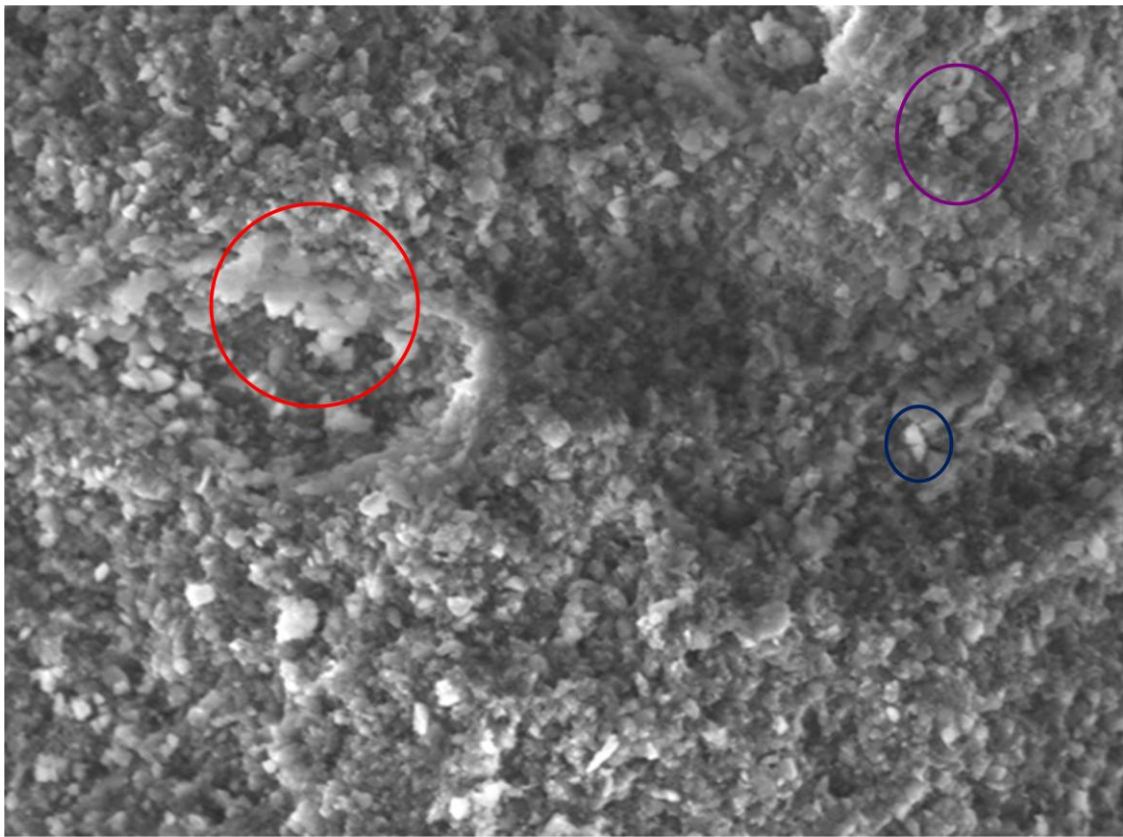
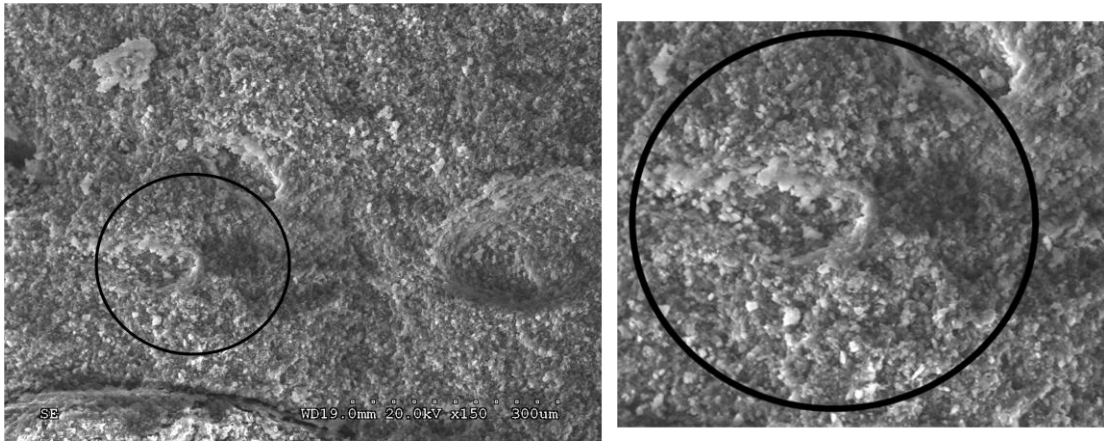


Figure 5-2: The bonding mechanisms that are present in sample 1.

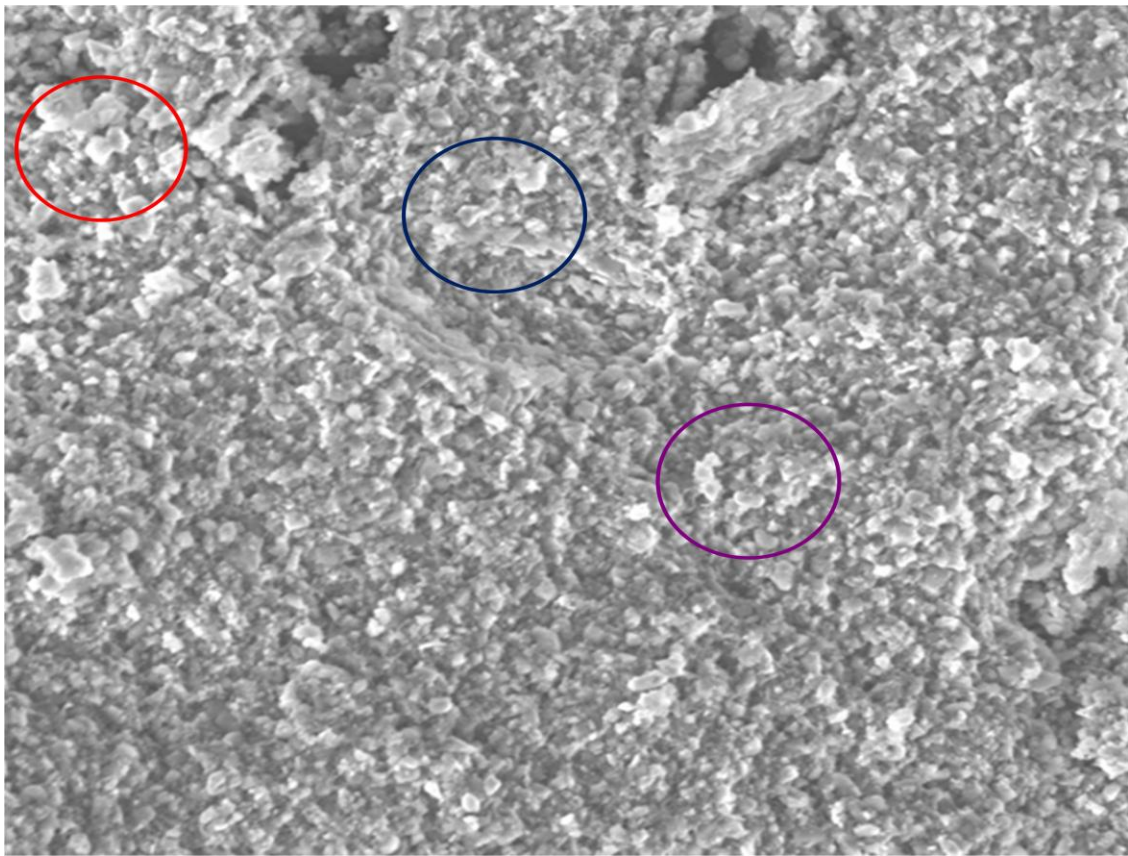
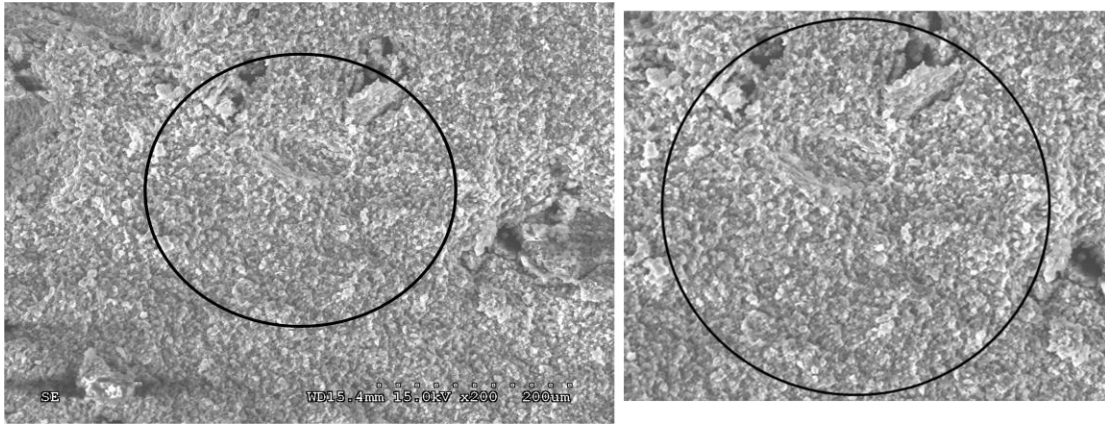


Figure 5-3: The bonding mechanisms that are present in sample 2.

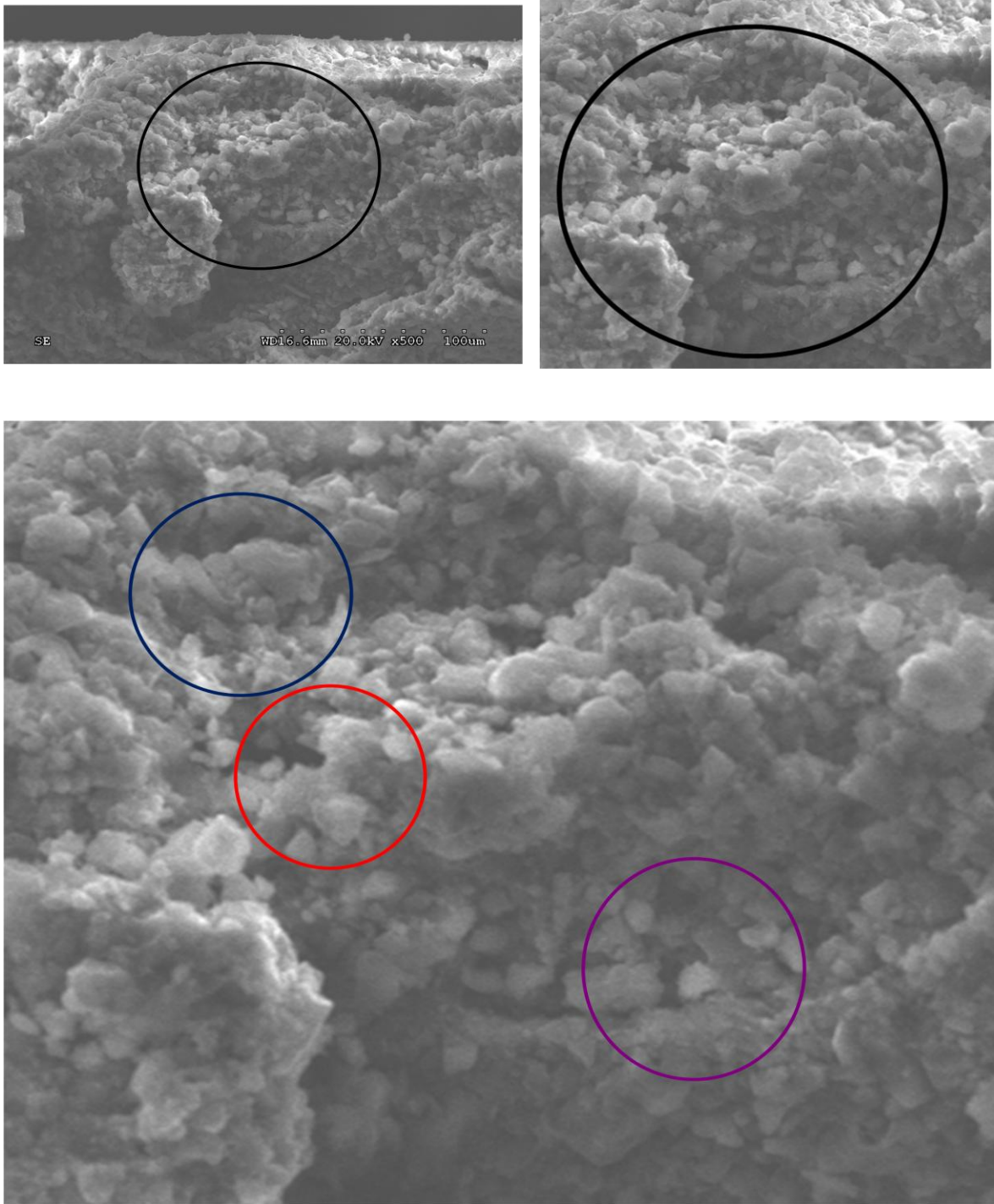


Figure 5-4: The bonding mechanisms that are present inside sample 3.

As the amount of erucamide in each sample increases it becomes easier to point out the mechanical bonding that takes place.

5.2 Thermal Conductivity

5.2.1 Thermal Conductivity Results

During pelletization, the press channel reaches temperatures close to 70-80°C. The temperatures applied to these experiments were also around this range. This provided the appropriate setting to see which material would be thermally activated and act as the heat transfer agent. Table 5-2 shows the measured thermal conductivities for the samples in Table 4-1. Figure 5-5 shows the linear relationship thermal conductivity has with the weight percent of erucamide. The results show with an increasing weight percent of erucamide, its ability to become more thermally activated increases. Thus, a larger amount of heat transfer occurs.

Table 5-2: The measured effective thermal conductivity obtained experimentally.

Sample:	Effective Thermal Conductivity (W/mK)
1	0.17
2	0.21
3	0.31
4	0.37

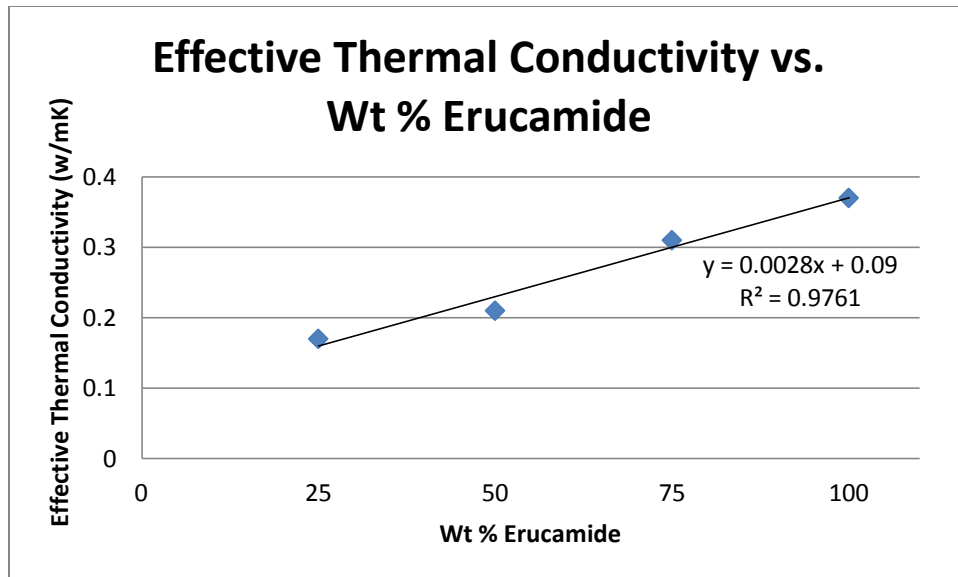


Figure 5-5: The change in thermal conductivity as the amount of erucamide increases.

Erucamide is a waxy material and will conduct heat throughout the sample as it softens during compaction. Therefore, it is likely to have a higher thermal conductivity. After an extensive literature search, the thermal conductivity of erucamide was not found. The inherent properties of erucamide are known; therefore, a comparison to a similar material, in order to determine if the experimentally calculated thermal conductivity of erucamide is accurate, can be made. Paraffin wax is a white and odorless waxy solid, there are anywhere from 20 to 40 carbons in its backbone, its typical melting point is 64°C, and the average density is 0.916 g/cm³ (17). According to Ukrainczyk the thermal conductivity of paraffin wax is 0.34 W/mK (17). Silica is a very porous, fine powder with a high melting temperature. Since the temperature in the process only reaches a maximum of 80°C, silica will not be thermally activated. Therefore, it is reasonable to assume that it will have a low thermal conductivity. According to Graves, pure precipitated silica has a thermal conductivity of 0.0043 W/mK (18).

The known values of thermal conductivity and the experimentally obtained values are very similar to each other. The standard deviation between these two values was found because it provides an absolute value between the positive and the negative difference. Erucamide's experimentally obtained value is 2% larger than the known value of paraffin wax; while silica's experimentally obtained value, 0.09 W/mK from equation in Figure 5-5, is 6% larger than the known value.

Figure 5-6 represents the thermal conductivity that was measured during the experiments. With a continual increase in temperature and maintained steady state, the thermal conductivity calculated was considered accurate since there's no variation.

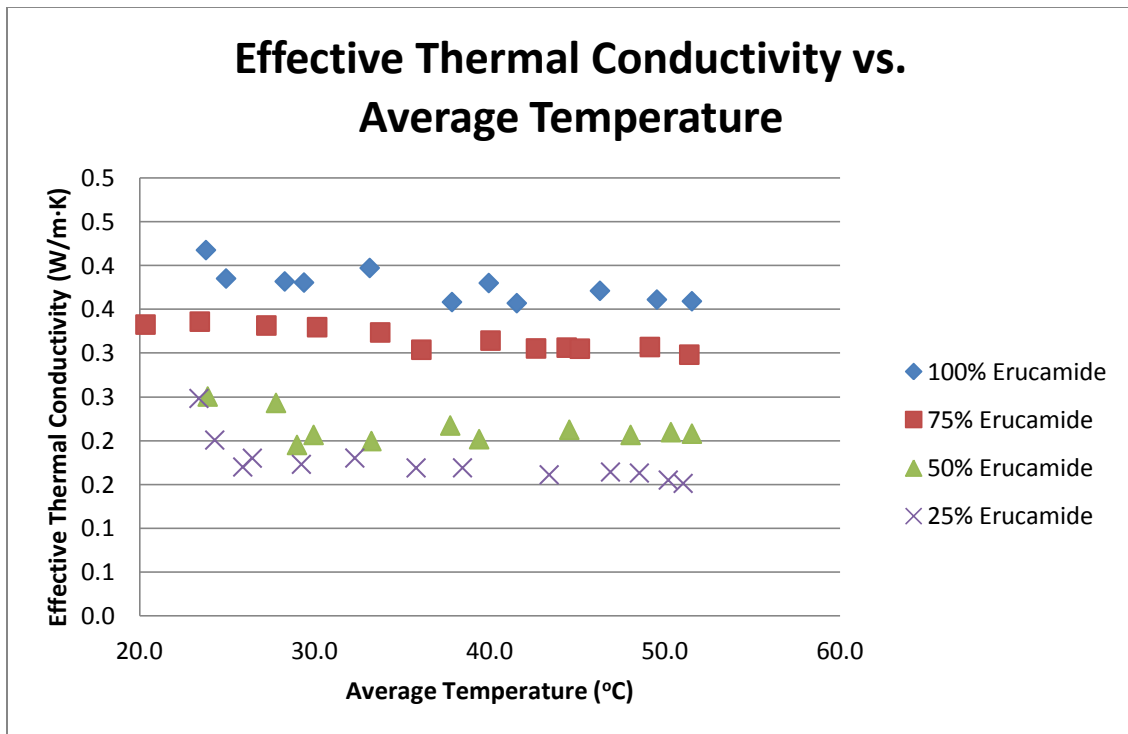


Figure 5-6: The effective thermal conductivity change as temperature increases.

5.2.2 Scanning Electron Microscope Results

Following the thermal conductivity experiments, it was important to characterize each sample using a scanning electron microscope (SEM). This provided critical insight

into how the heat affected the top of each sample closest to the heating element. Figure 5-7 shows how the heat was transferred into the sample. Figure 5-7a shows sample 4 with the largest penetration depth. The penetration depth decreases as the weight percent of silica increases because heat transfer becomes hindered.

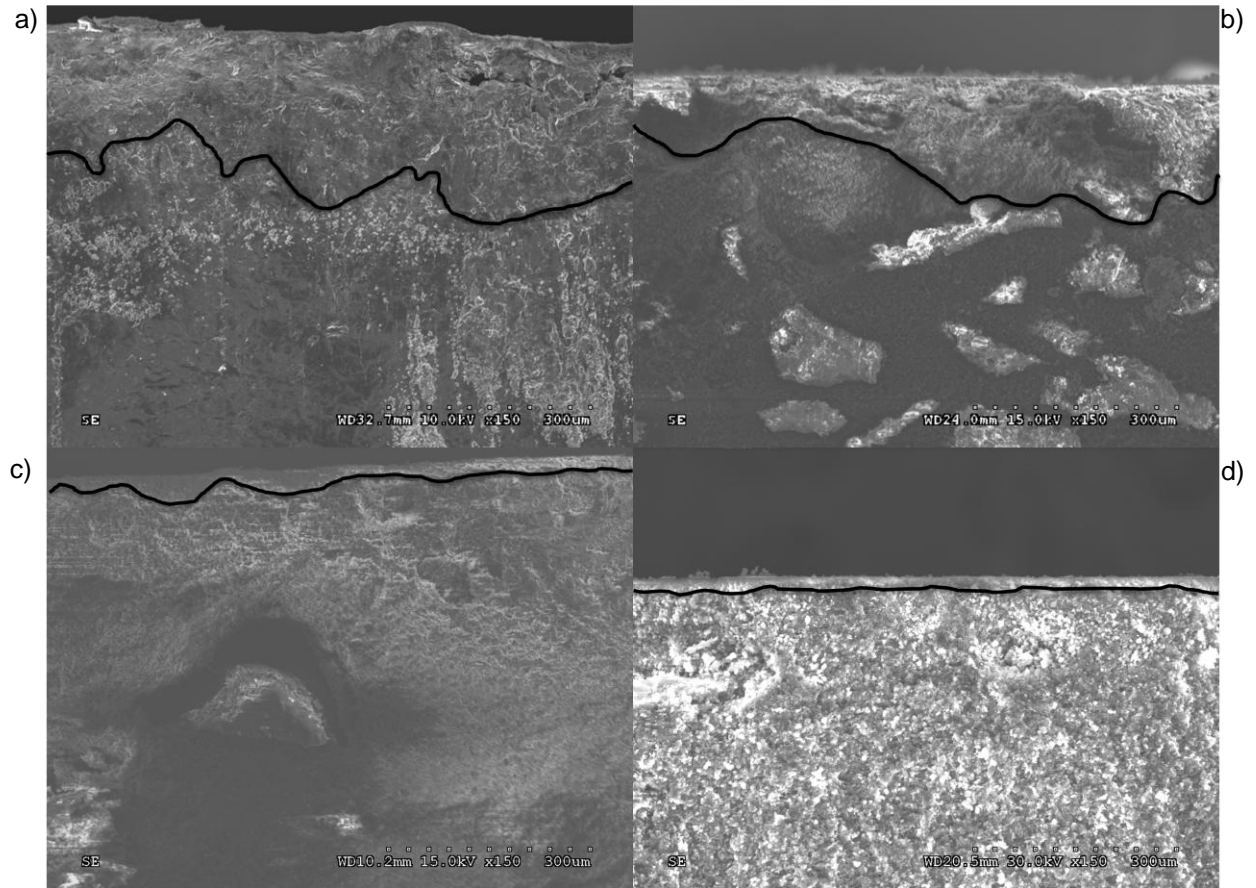


Figure 5-7: The SEM micrographs of a) sample 4, b) sample 3, c) sample 2, and d) sample 1.

From Figure 5-7, a penetration depth was measured to see how the depth was affected by decreasing the weight percent of erucamide. Table 5-3 shows the calculated penetration depth from each micrograph. Figure 5-8 shows the linear correlation between

the penetration depth and the weight percent of erucamide from each sample. Thus, providing evidence that erucamide acts as the heat transfer agent.

Table 5-3: The measured penetration depth that evolved through the effective thermal conductivity experiments.

Sample:	Penetration Depth (μm):
4	245
3	136
2	54
1	14

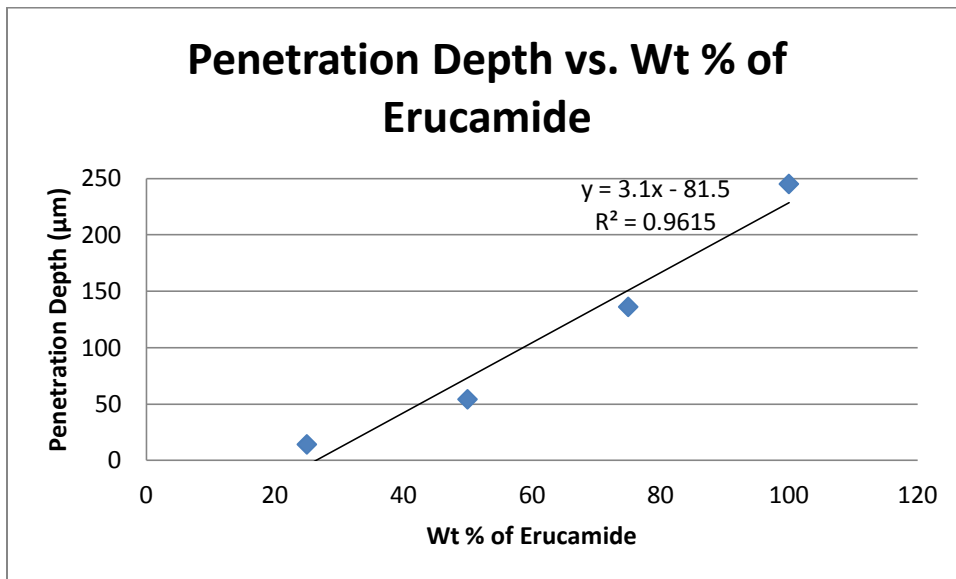


Figure 5-8: The penetration depth vs. wt % of erucamide that was measured.

5.2.3 Energy-Dispersive Spectroscopy

Energy-dispersive spectroscopy was utilized in order to understand how compaction combined silica and erucamide. Figure 5-9 shows how sample 1 was combined into a solid compacted disc.

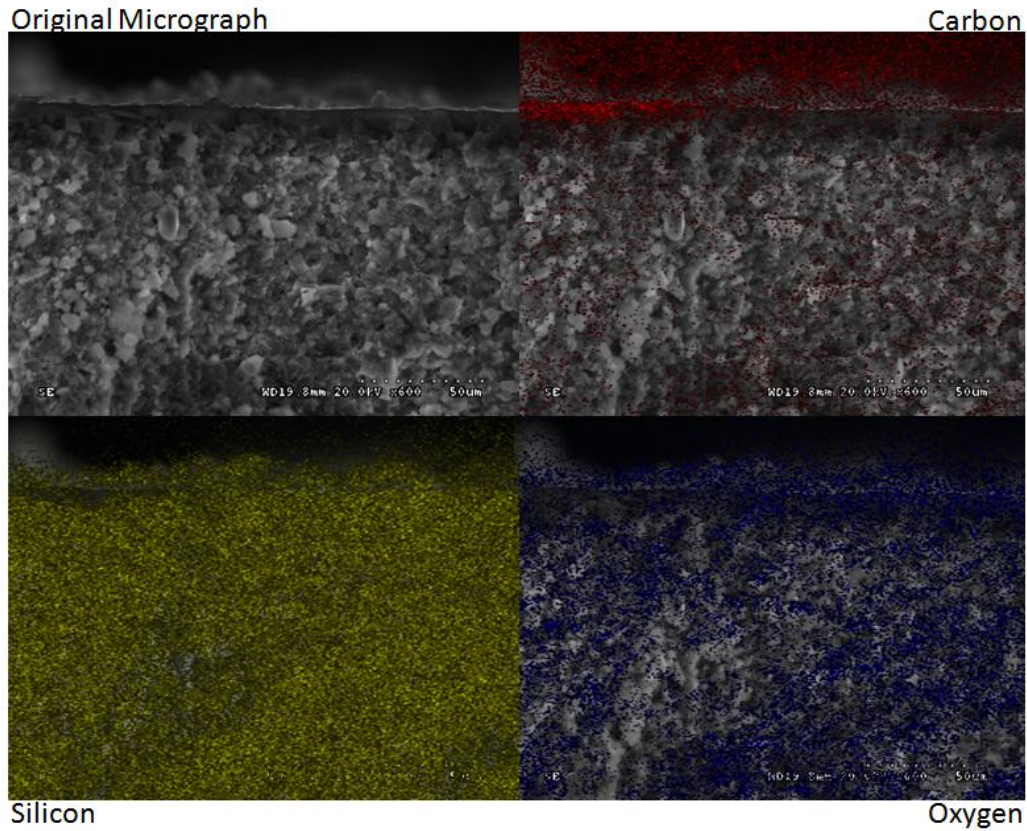


Figure 5-9: The original micrograph and elemental mapping for sample 1.

Table 5-4 shows the elemental percent of silicon, carbon, and oxygen present in the compacted sample. The percentage of silicon and oxygen present in the sample is large because the sample's composition is primarily silica. There is a small amount of carbon present because erucamide makes up only twenty-five percent of the sample.

Table 5-4: The elemental weight percent of silicon, carbon, and oxygen in sample 1.

Element:	Wt %:
Carbon	45.36
Oxygen	37.93
Silicon	14.95

Figure 5-10 shows how sample 2 was combined to form a solid compacted disc. From the micrograph one is able to see that there is an even distribution of silicon, carbon, and oxygen present in the sample.

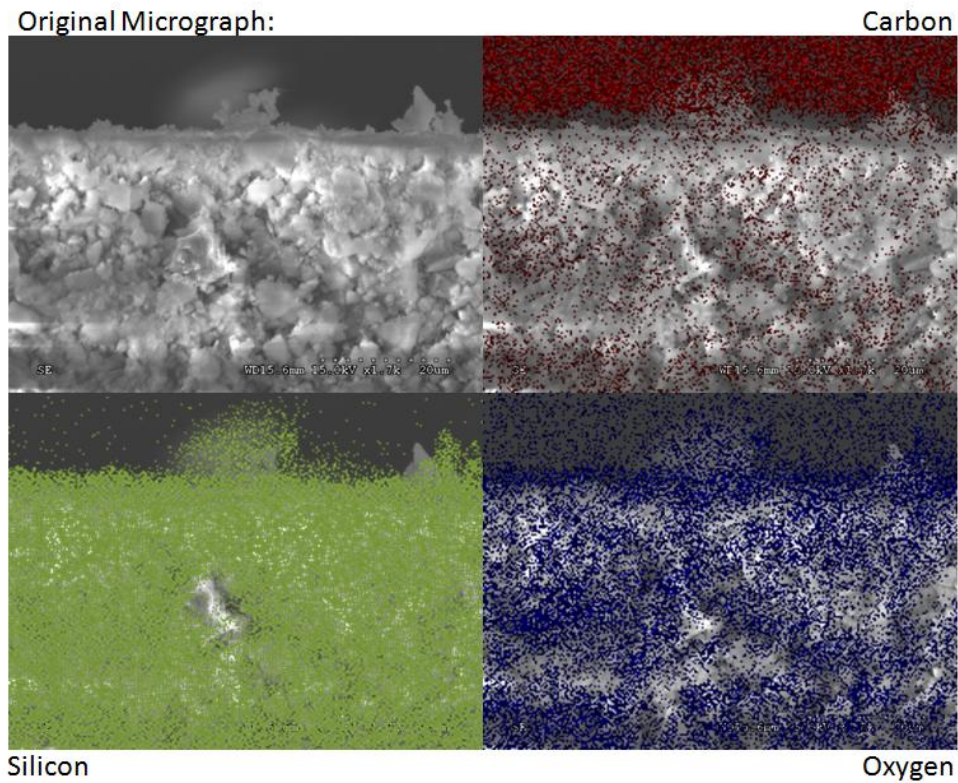


Figure 5-10: The original micrograph and elemental mapping for sample 2.

Table 5-5 shows the elemental percent of silicon, carbon, and oxygen present in the compacted sample. Silicon and oxygen make up fifty percent of the composition since silica makes up half of the composition. Erucamide makes up the other fifty percent of the compacted disc, so having a large elemental weight percent of carbon is expected.

Table 5-5: The elemental weight percent of silicon, carbon, and oxygen in sample 2.

Element:	Wt %:
Carbon	51.36
Oxygen	30.08
Silicon	18.56

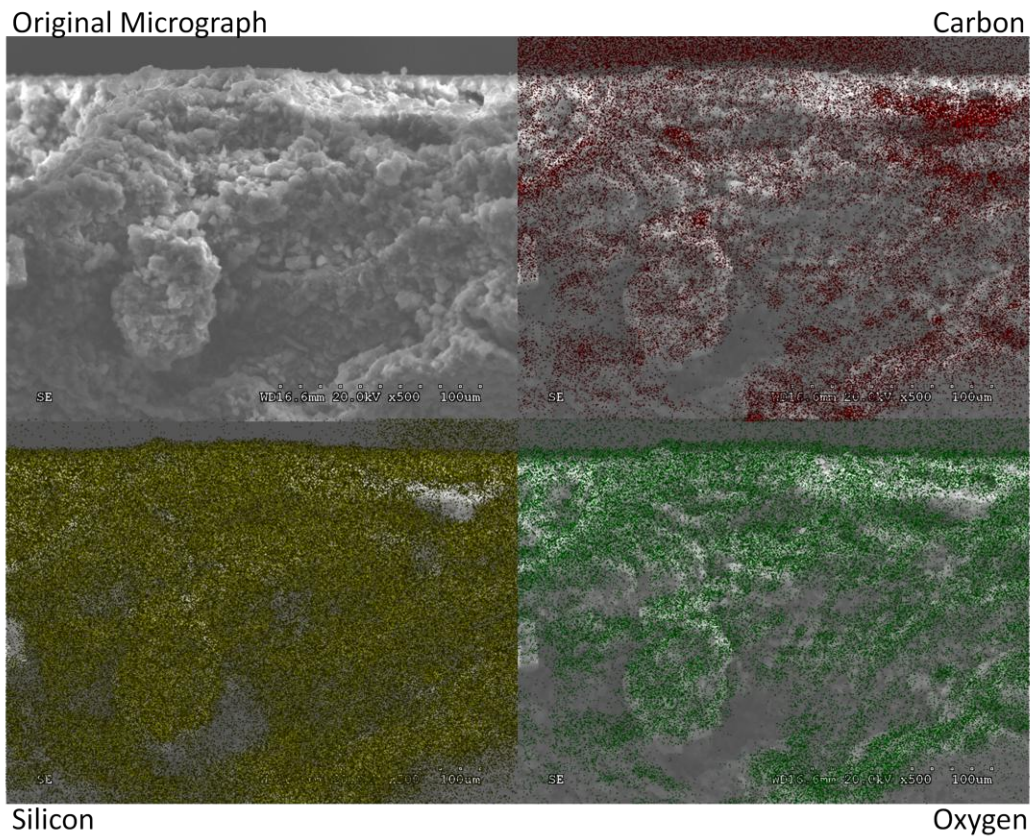


Figure 5-11: The original micrograph and elemental mapping for sample 3.

Table 5-6 shows the elemental percent of silicon, carbon, and oxygen present in the compacted sample. The elemental weight percentage of silicon and oxygen present in the sample is smaller than fifty percent since silica only makes up twenty-five percent of the sample's composition. The large amount of carbon present in the sample is due to erucamide which makes up seventy-five percent of the sample's composition.

Table 5-6: The elemental weight percent of silicon, carbon, and oxygen in sample 3.

Element:	Wt %:
Carbon	58.32
Oxygen	30.42
Silicon	11.25

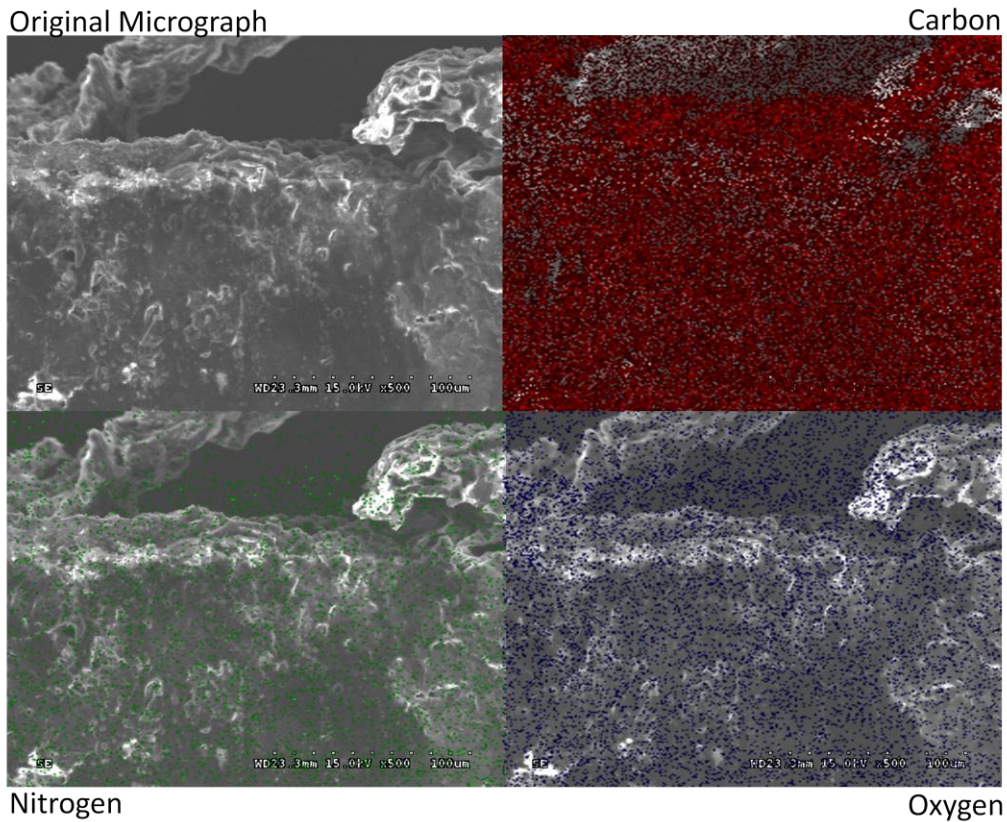


Figure 5-12: The original micrograph and elemental mapping for sample 4

Table 5-7 shows the elemental percent of nitrogen, carbon, and oxygen present in the compacted sample. The elemental weight percentage is based only on erucamide. Therefore carbon makes up most of the sample since erucamide is made up of a long chain carbon back-bone. A small percentage comes from nitrogen and oxygen which comes from the amide group hanging off the long chain carbon back-bone.

Table 5-7: The elemental weight percent of silicon, carbon, and oxygen in sample 4.

Element	Wt %
Carbon	78.86
Nitrogen	9.13
Oxygen	12.01

5.3 Frictional Heating

5.3.1 Tribometer Testing

The tribological tests for samples 1, 2, and 3 shows how the friction coefficient changes as the amount of erucamide increases in each sample. Silica is known as an anti-blocking agent; therefore, as the amount of silica increases so does the friction coefficient because it becomes harder for flow to occur. According to Thongsang et al the coefficient of friction was found to be around 0.75 (19). As the amount of erucamide increases in each compacted disc, the friction coefficient will decrease because erucamide is known as a slip additive. A slip additive helps with flow thus decreasing the amount of friction that occurs in the system. According to Maltby et al and Ramírez et al the coefficient of friction was found to be 0.2 (20; 21).

The experimental conditions that were used for samples 1, 2, and 3 are shown in Table 5-8. For each sample the amount of laps and load vary in order to understand how these variables affect the heat generation depth. The micrographs for each experimental test are shown below.

Table 5-8: The different experiments that were conducted using the tribometer.

Sample:	Radius (mm):	Laps:	Linear Speed (cm/sec):	Load (N):
1	8	200	10	2
1	11	100	10	2
1	19	250	10	1
2	10	50	10	2
2	15	20	10	1
2	20	24	10	2
3	15	300	10	1
3	17	20	10	2
3	20	500	10	1

5.3.1.1 25% Erucamide- 75% Silica (Sample 1)

Figure 5-13, Figure 5-15, and Figure 5-17 show the heat penetration depth that occurred during each tribological experiment. The penetration depth for each sample varied with the 8mm radius having a depth of 260 μ m, the 11mm radius having a depth of 41 μ m, and the 19mm radius having a depth of 88 μ m. Figure 5-14, Figure 5-16, and Figure 5-18 show the diameter of the pin that touched the sample. The diameter of each sample varied depending on the amount of load and the number of laps that each test ran. When a higher load was applied to the sample a longer wear track was formed; however, when the when a higher load but lower amount of laps matched a lower load with a higher amount of laps the length of the wear track was very similar as seen in Figure 5-16 and Figure 5-18. However, the heat penetration for each sample was different.

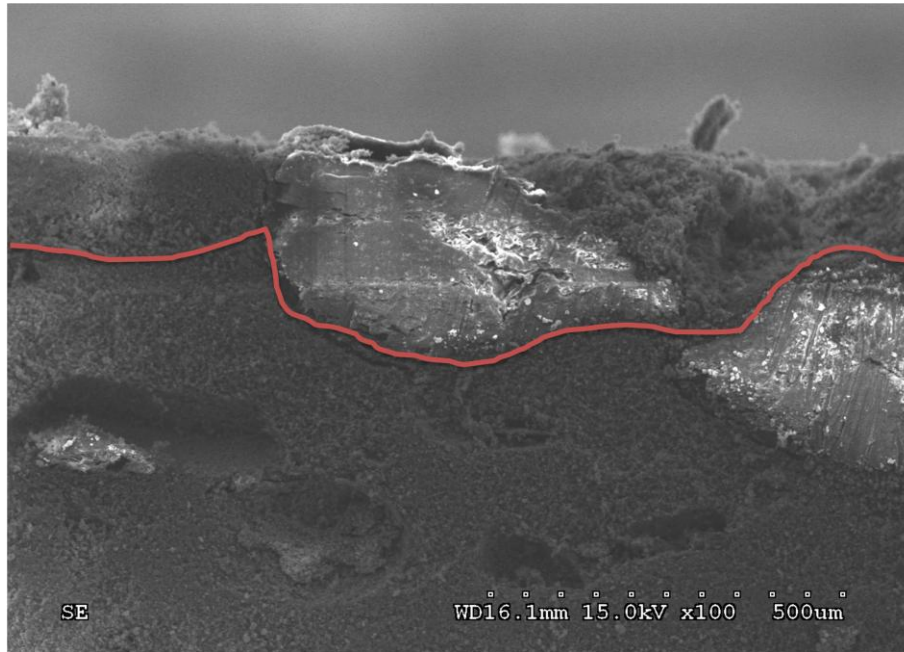


Figure 5-13: The SEM micrograph showing the formation of a softened area at a 8mm radius.

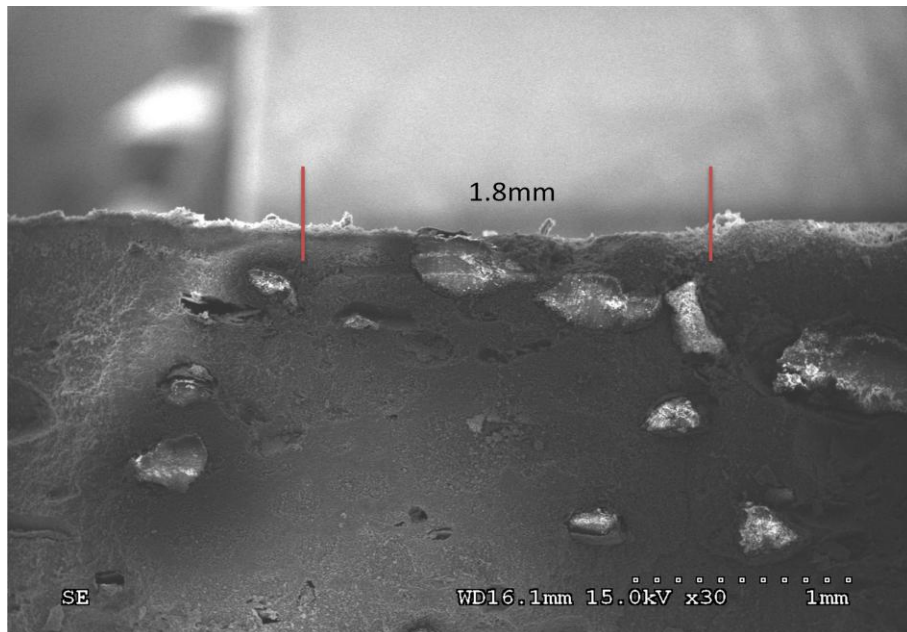


Figure 5-14: The diameter of the wear track made by the pin.

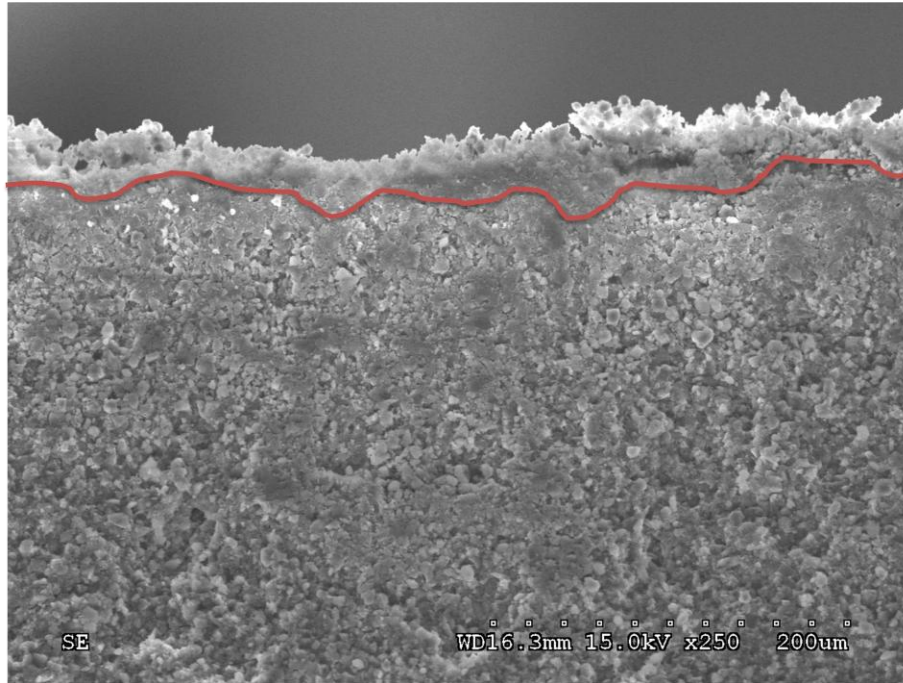


Figure 5-15: The SEM micrograph showing the formation of a softened area at a 11mm radius.

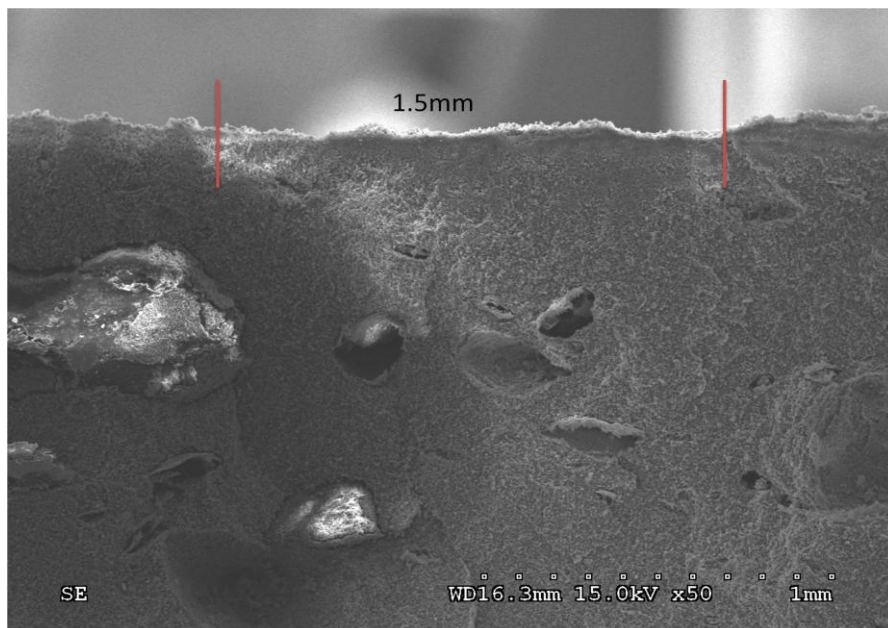


Figure 5-16: The diameter of the wear track made by the pin.

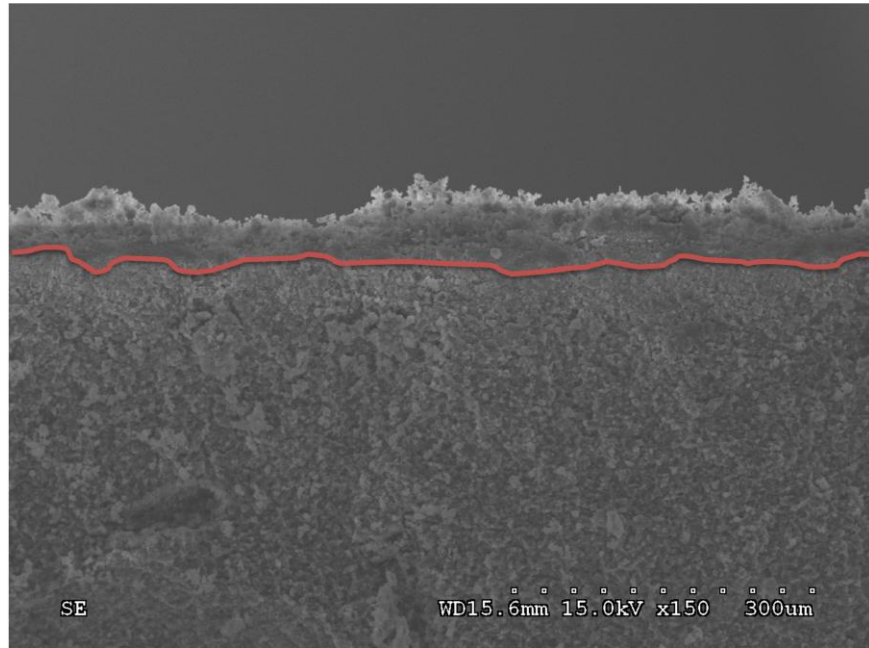


Figure 5-17: The SEM micrograph showing the formation of a softened area at a 19mm radius.

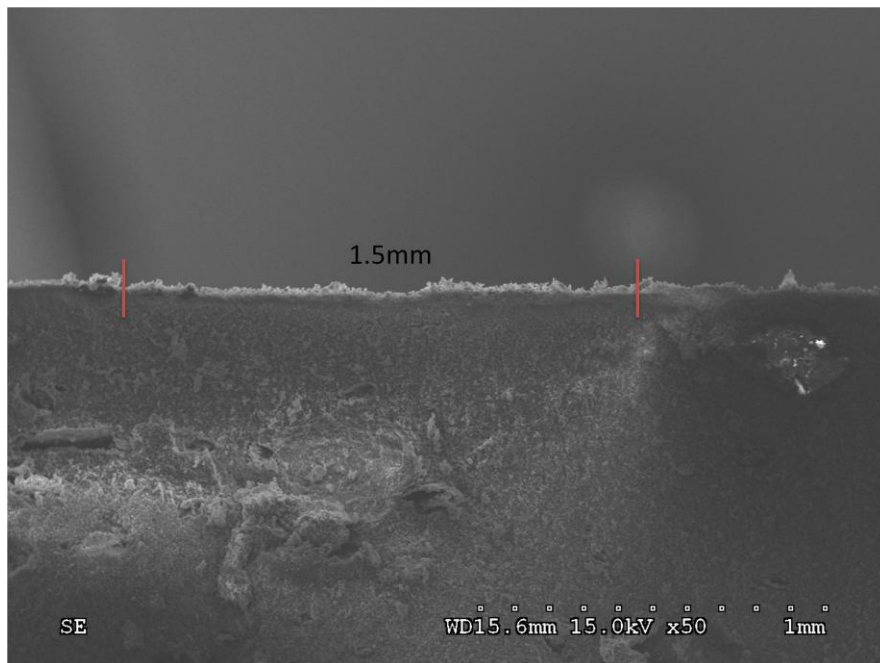


Figure 5-18: The diameter of the wear track made by the pin.

Figure 5-19, Figure 5-20, and Figure 5-21 show the measured coefficient of friction during each tribological test. Figure 5-19 and Figure 5-20 show the coefficient of friction that was obtained using a 2N load. The amount of laps varied between each test, and it was seen that the test with the higher amount of laps applied has a higher coefficient of friction. This was due to a large amount of silica being present around the 8mm radius area. When there is a large amount of silica a high coefficient of friction will occur due its anti-blocking properties. Figure 5-20 and Figure 5-21 represent the coefficient of friction obtained using different loads and varied lap amounts. When a lighter load is applied onto the sample, thermal activation of erucamide becomes hindered and a higher coefficient of erucamide is measured. Figure 5-19 shows the most accurate coefficient of friction for this particular blend due to its ability to activate erucamide even though the weight percent of silica is very high.

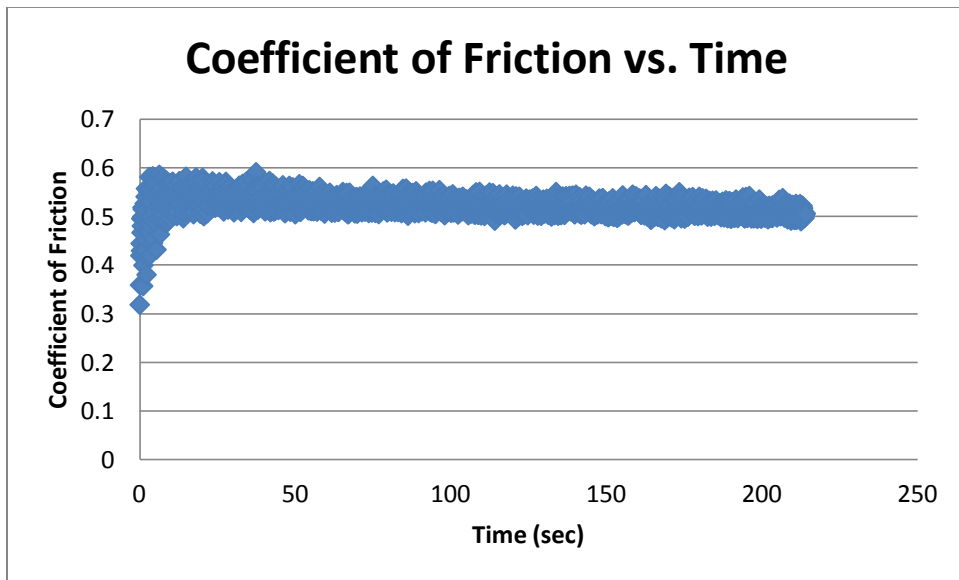


Figure 5-19: The measured coefficient of friction for the 8mm radius.

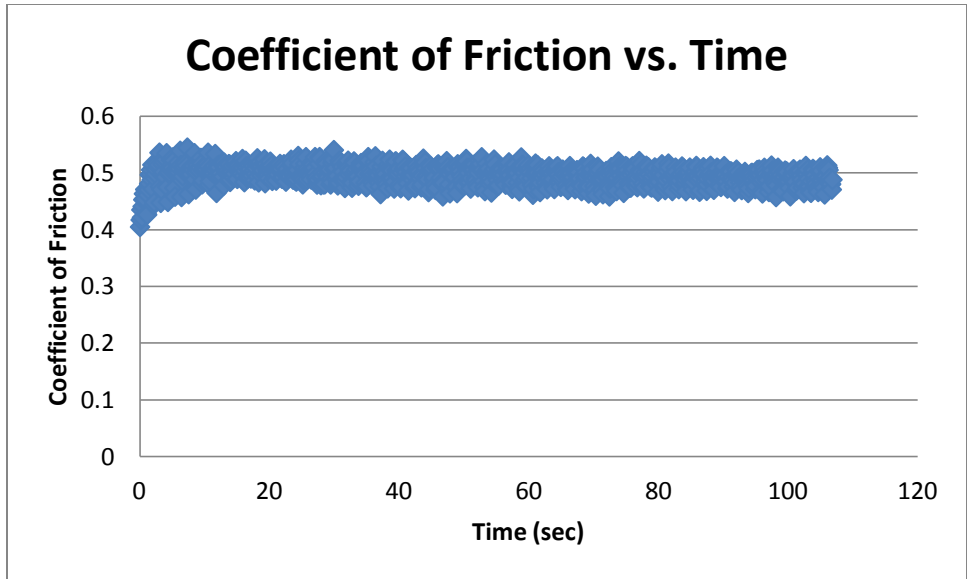


Figure 5-20: The measured coefficient of friction for the 11mm radius.

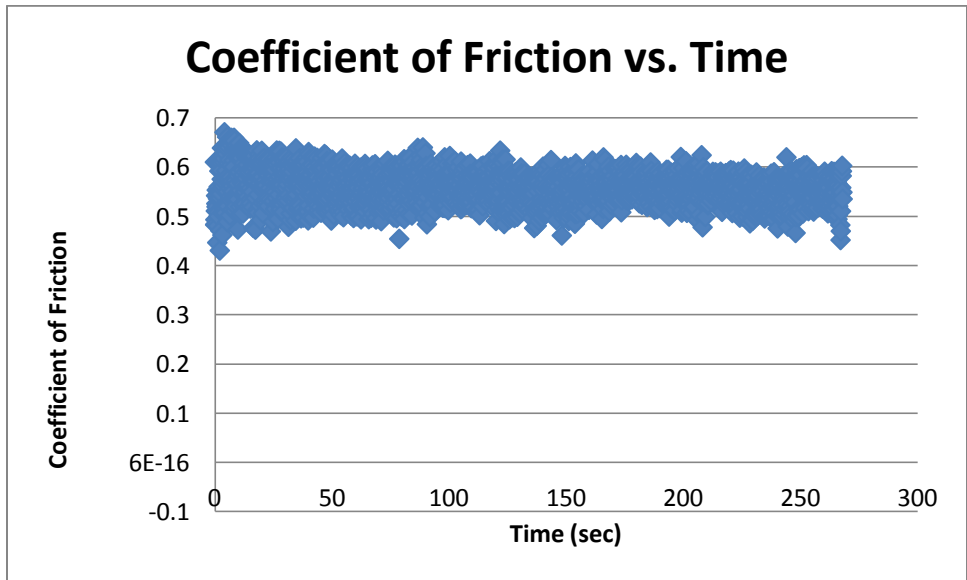


Figure 5-21: The measured coefficient of friction for the 19mm radius.

Figure 5-22, Figure 5-23, and Figure 5-24 show the relationship that temperature has with depth during sample 1's frictional heating experiments. During each experiment, a critical depth was achieved. It can be seen on each of the following graphs that a

dashed line shows that critical depth and how it corresponds to a critical temperature for different radius lengths. Figure 5-22 shows the highest critical depth and the lowest critical temperature, this is due to the experiment running at such a small radius. The cooling time in-between rotations of the pin were greatly decreased allowing for more heat to evolve and a greater penetration depth. Figure 5-23 and Figure 5-24 show differing critical depths; however, the critical temperature that was reached during these separate experiments to achieve these depths is the same.

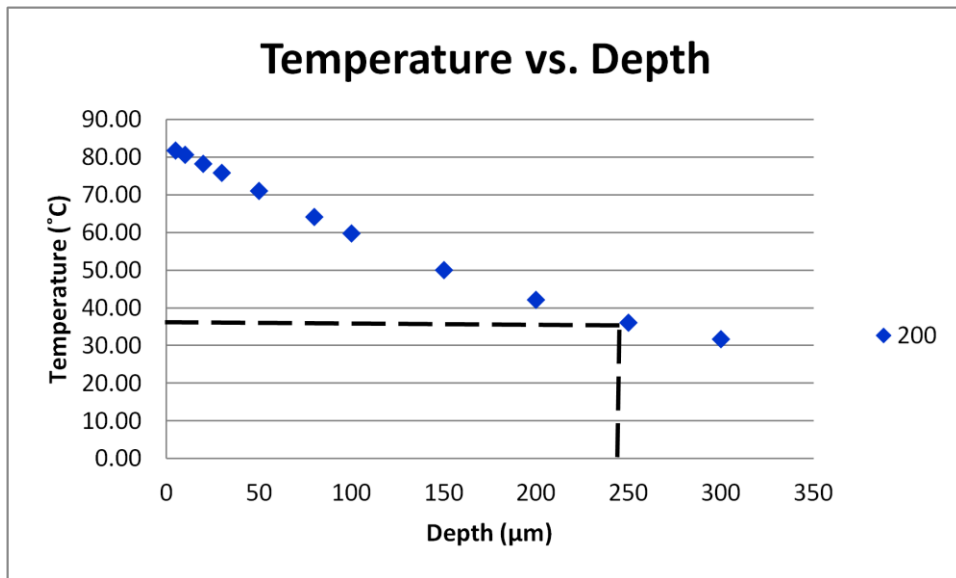


Figure 5-22: The relationship between temperature and depth for 8mm radius.

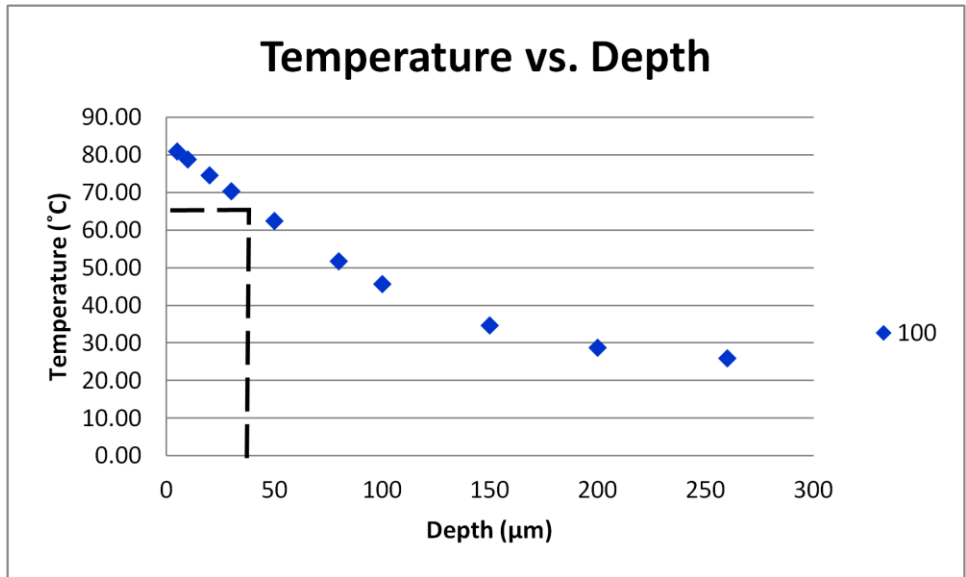


Figure 5-23: The relationship between temperature and depth for 11mm radius.

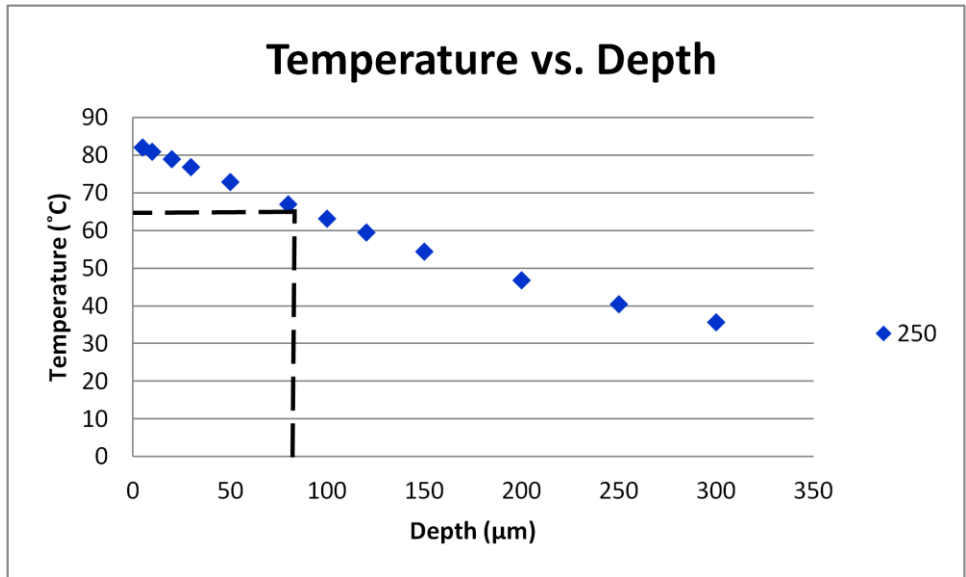


Figure 5-24: The relationship between temperature and depth for 19mm radius.

5.3.1.2 50% Erucamide- 50% Silica (Sample 2)

Figure 5-25, Figure 5-27, and Figure 5-29 show the heat penetration depth that occurred during each tribological experiment. The penetration depth for each sample varied with the 10mm radius having a depth of 81 μm , the 15mm radius having a depth of 27 μm , and the 20mm radius having a depth of 54 μm . Figure 5-26, Figure 5-28, and Figure 5-30 show the diameter of the pin that touched the sample. The diameter of each sample varied depending on the amount of load and the number of laps that each test ran. When a higher load was applied to the sample a longer wear track was formed.

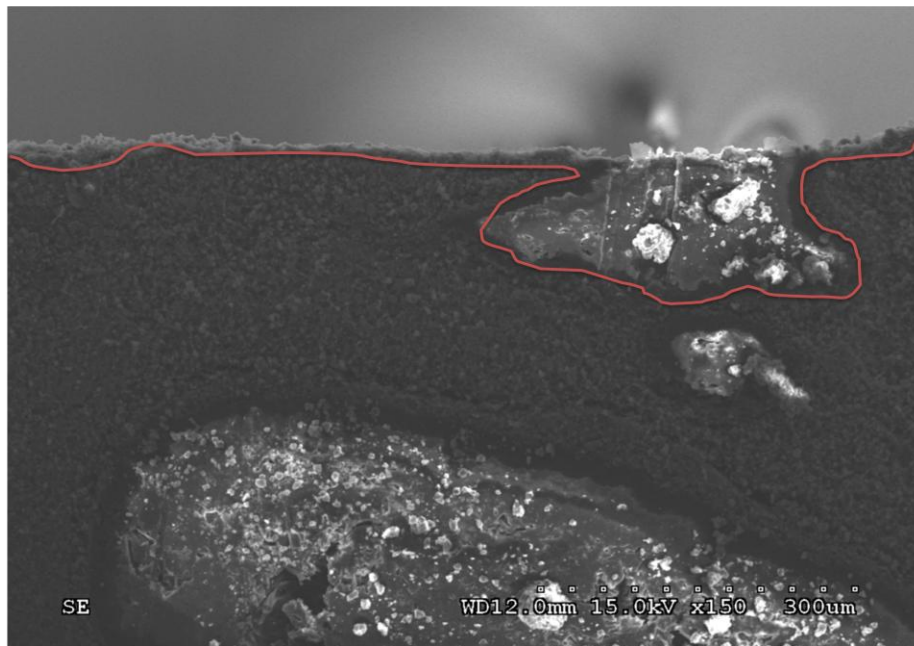


Figure 5-25: The SEM micrograph showing the formation of a softened area at a 10mm radius.

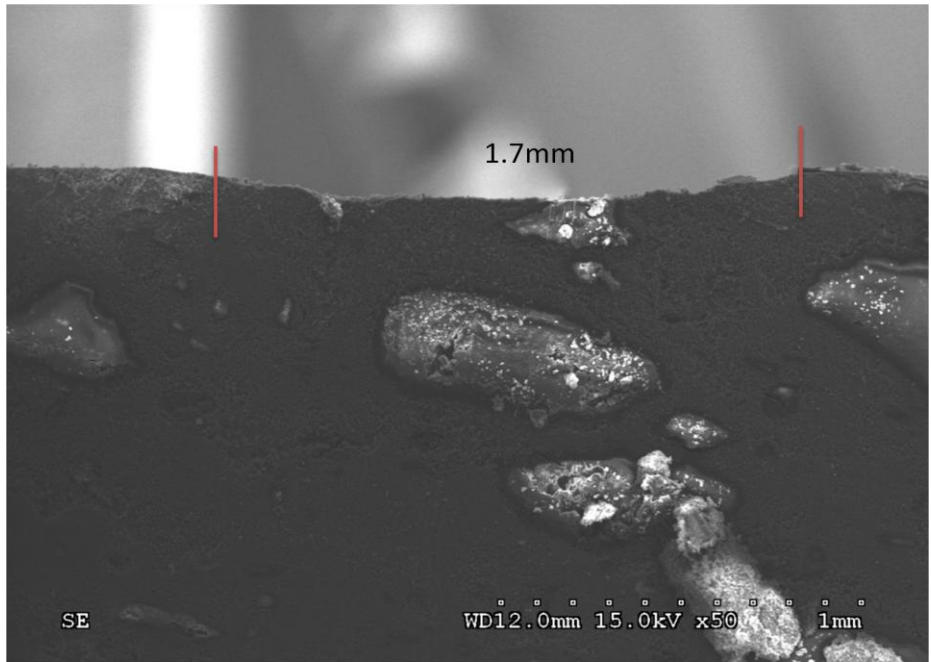


Figure 5-26: The diameter of the wear track made by the pin.

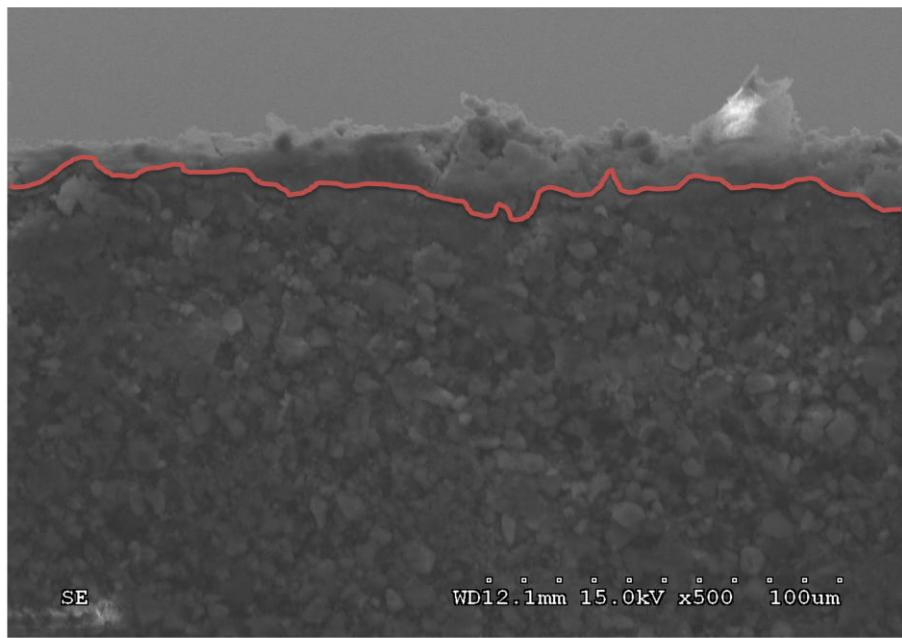


Figure 5-27: The SEM micrograph showing the formation of a softened area at a 15mm radius.

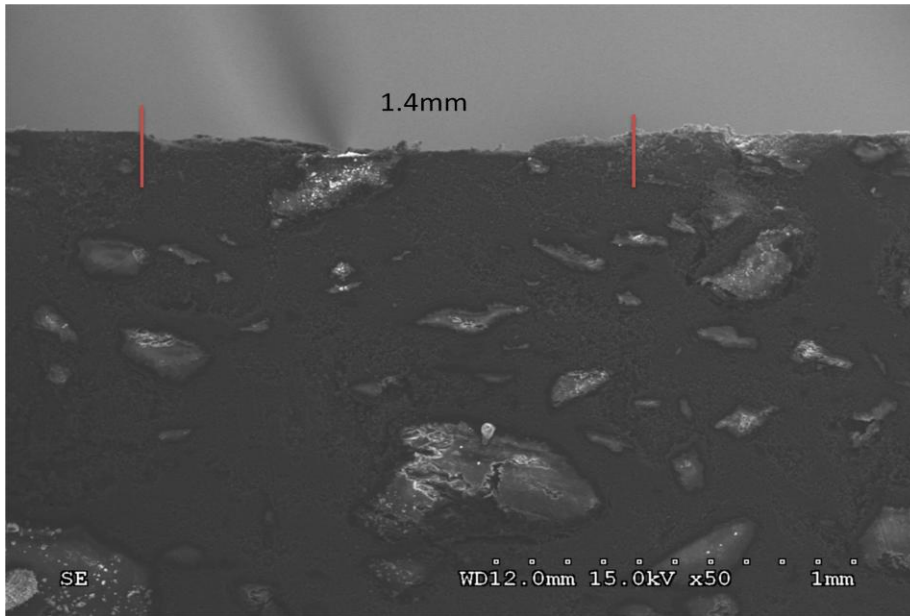


Figure 5-28: The diameter of the wear track made by the pin.

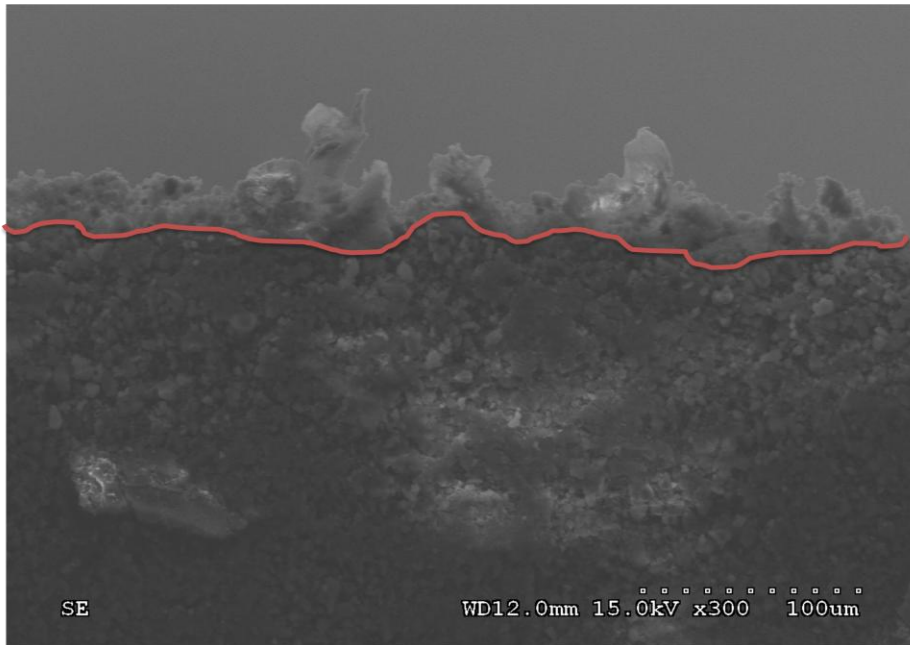


Figure 5-29: The SEM micrograph showing the formation of a softened area at a 20mm radius.

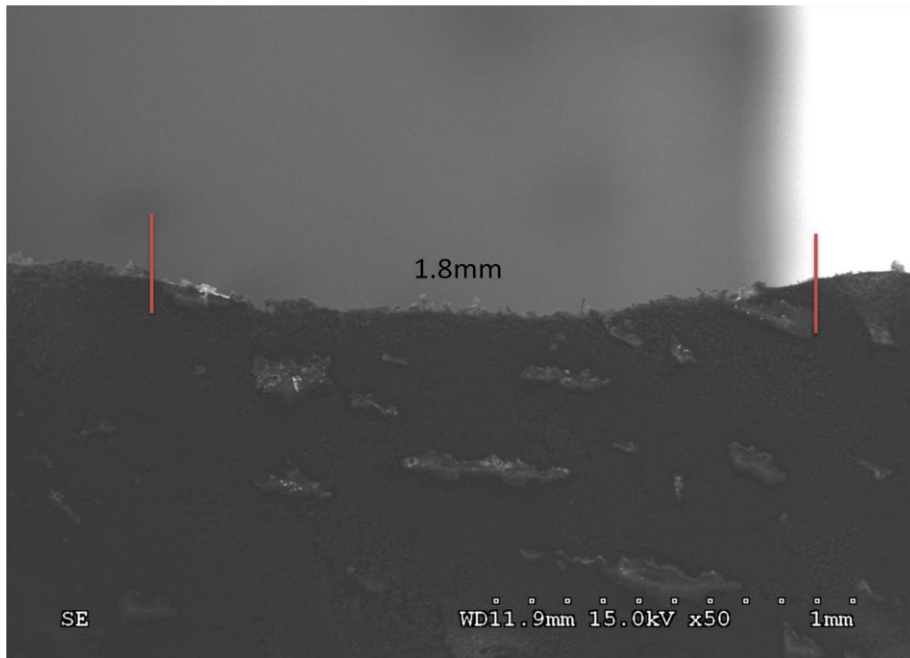


Figure 5-30: The diameter of the wear track made by the pin.

Figure 5-31, Figure 5-32, and Figure 5-33 show the measured coefficient of friction during each tribological test. Figure 5-31 and Figure 5-33 show the coefficient of friction that was obtained using a 2N load. The amount of laps varied between each test, and it was seen that the test with the higher amount of laps applied had a lower coefficient of friction. This is due to the erucamide, a slip additive, becoming thermally activated since a large load with a high amount of laps was applied. Figure 5-31 and Figure 5-32 represent the coefficient of friction obtained using different loads and varied lap amounts. When a lighter load is applied onto the sample, thermal activation of erucamide can become hindered because the amount of pressure applied to create heat is too low. This causes a higher coefficient of friction to be measured. Figure 5-31 has the most extended experiment for this particular blend; therefore provides the most accurate coefficient of friction for this particular weight percent of erucamide.

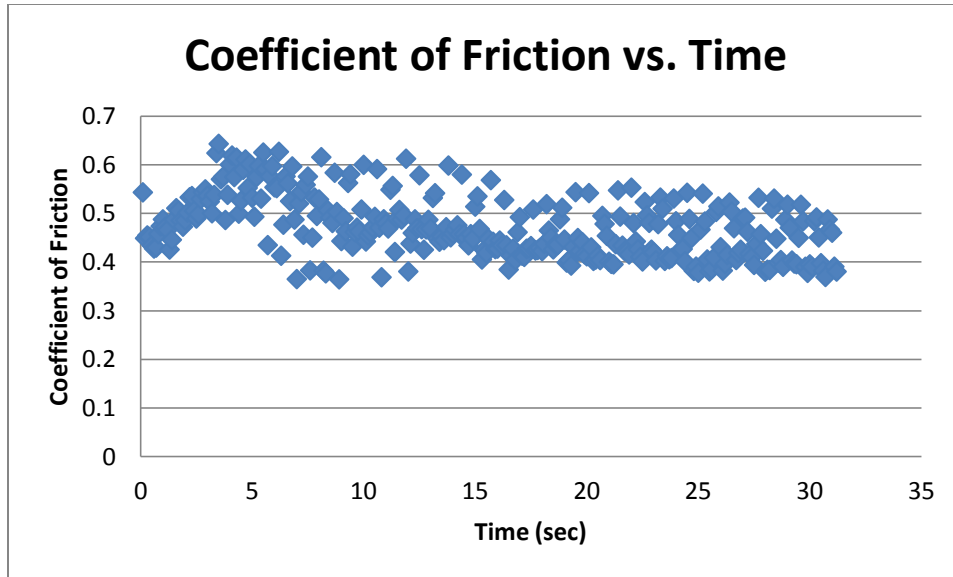


Figure 5-31: The coefficient of friction for the 10mm radius.

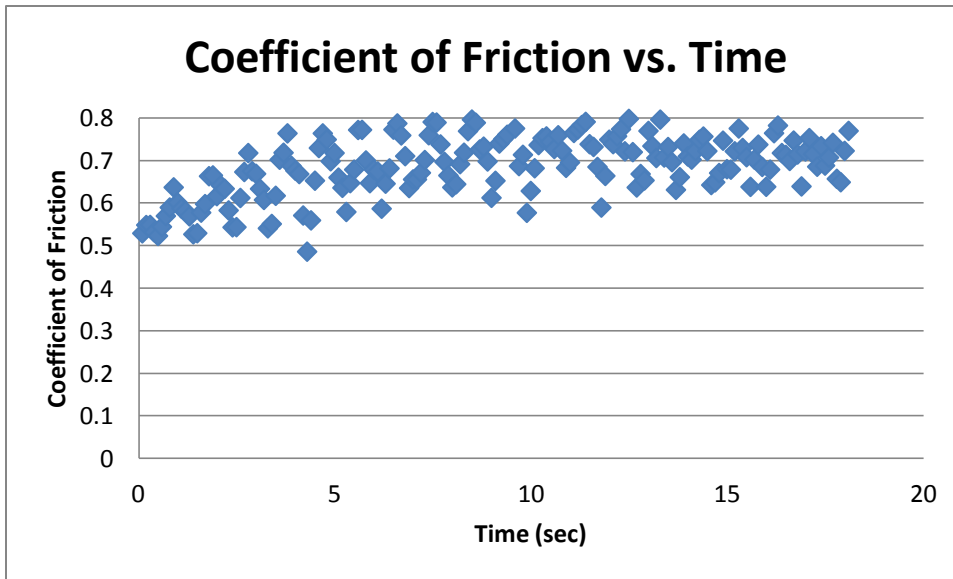


Figure 5-32: The coefficient of friction for the 15mm radius.

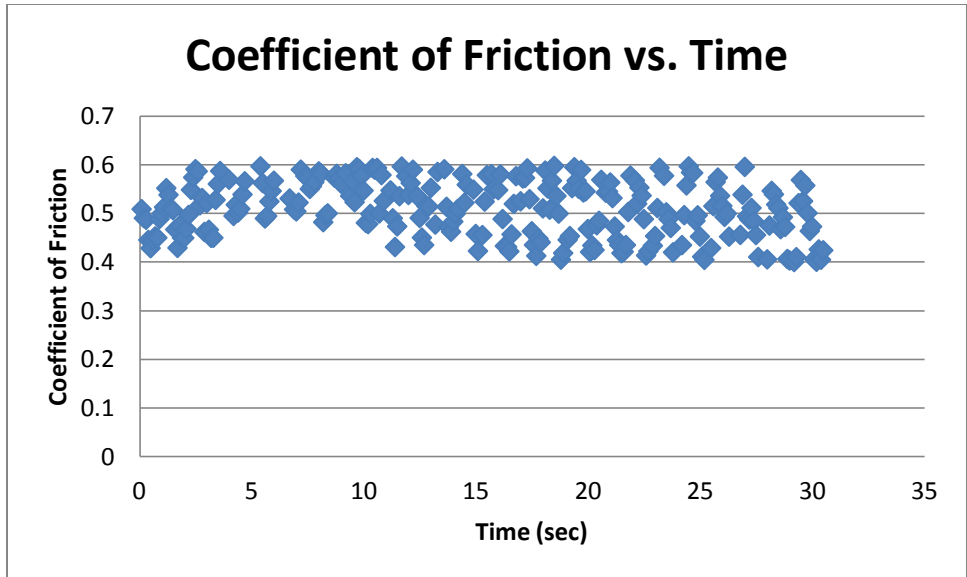


Figure 5-33: The coefficient of friction for the 20mm radius.

Figure 5-34, Figure 5-35, and Figure 5-36 show the relationship that temperature has with depth during sample 2's frictional heating experiments. During each experiment, a critical depth was achieved which is highlighted on each graph with a dashed line. This critical depth corresponds to a critical temperature at which this depth will be achieved. Figure 5-34 shows the highest critical depth and the lowest critical temperature, this is due to the experiment running at such a small radius. The cooling time in-between rotations of the pin were greatly decreased allowing for more heat to evolve and a greater penetration depth. Figure 5-35 and Figure 5-36 show differing critical depths; however, the critical temperature that was reached during these separate experiments to achieve these depths is the same.

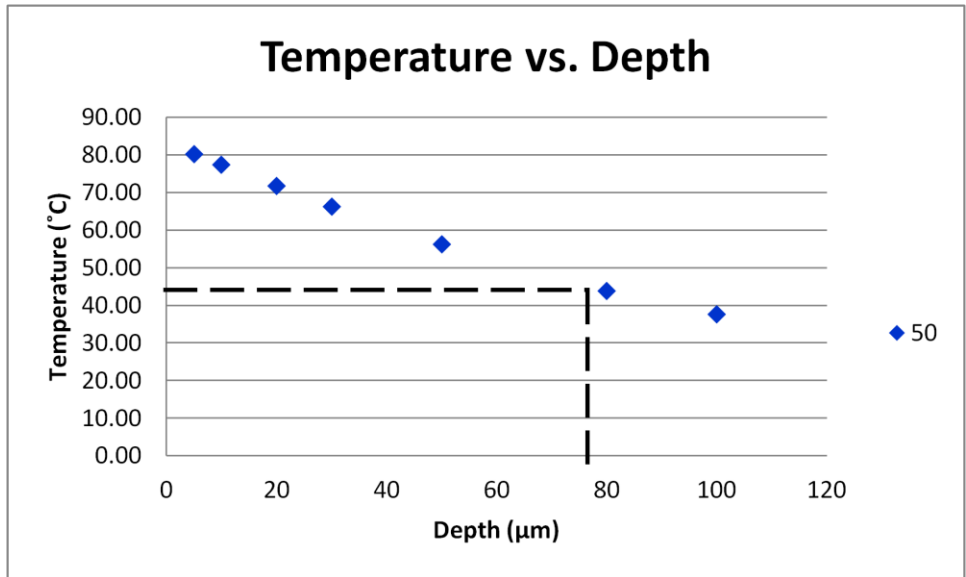


Figure 5-34: The relationship between temperature and depth for 10mm radius.

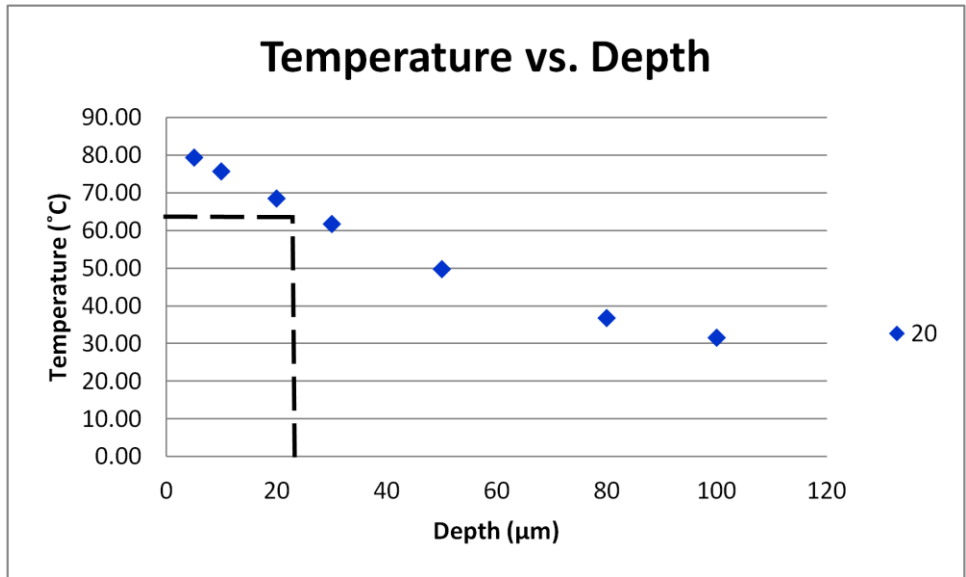


Figure 5-35: The relationship between temperature and depth for 15mm radius.

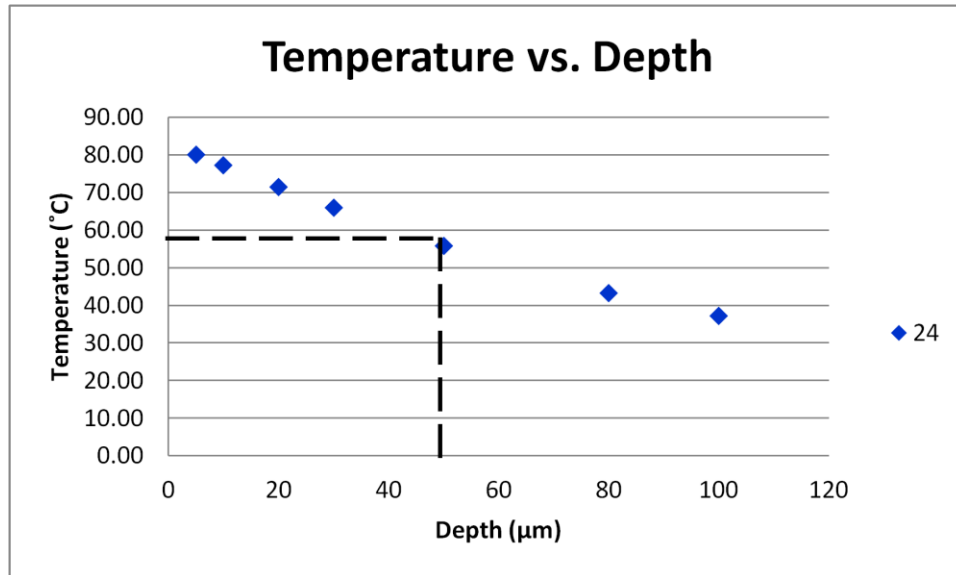


Figure 5-36: The relationship between temperature and depth for 20mm radius.

5.3.1.3 75% Erucamide-25% Silica (Sample 3)

Figure 5-37, Figure 5-39, and Figure 5-41 show the heat penetration depth that occurred during each tribological experiment. The penetration depth for each sample varied with the 15mm radius having a depth of 111 µm, the 17mm radius having a depth of 36 µm, and the 20mm radius having a depth of 177 µm. Figure 5-38, Figure 5-40, and Figure 5-42 show the diameter of the pin that touched the sample. The diameter of each sample varied depending on the amount of load and the number of laps that each test ran. Figure 5-40 shows the smallest diameter attained for these experiments. Although the load applied during this experiment was higher than for the other two experiments; the amount of laps ran was exceedingly lower. Therefore, the experiment was not long enough for the pin to penetrate the surface to leave a large diameter wear track. The length of the wear tracks had to be determined from the planar view due to the elastic property that erucamide has.

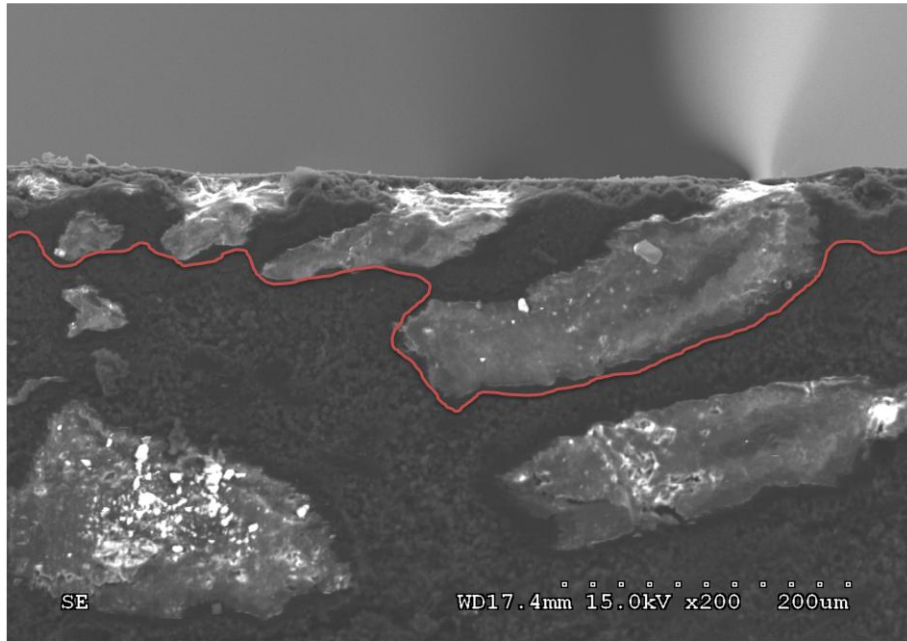


Figure 5-37: The SEM micrograph showing the formation of a softened area at a 15mm radius.



Figure 5-38: The diameter of the wear track made by the pin.



Figure 5-39: The SEM micrograph showing the formation of a softened area at a 17mm radius.

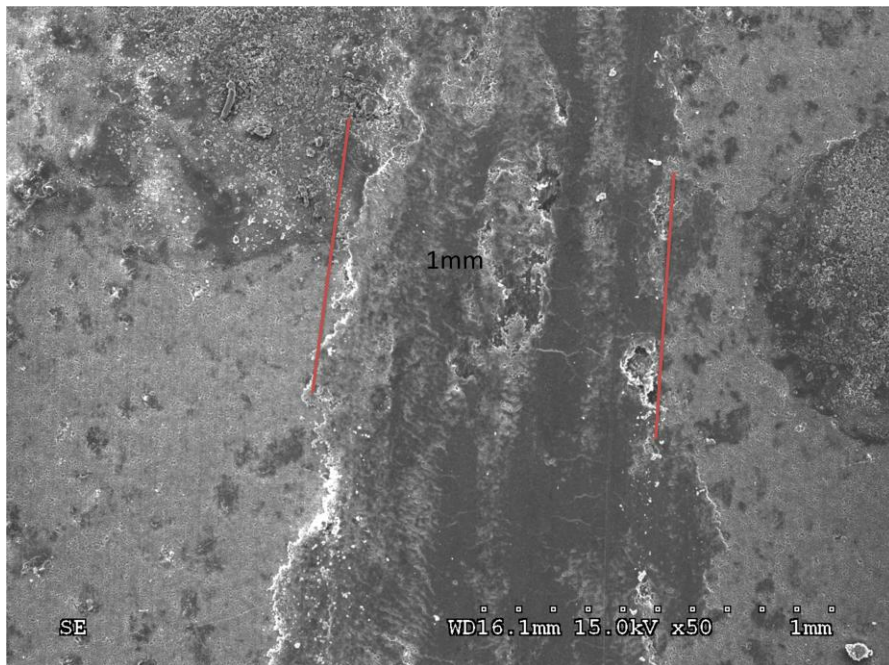


Figure 5-40: The diameter of the wear track made by the pin.

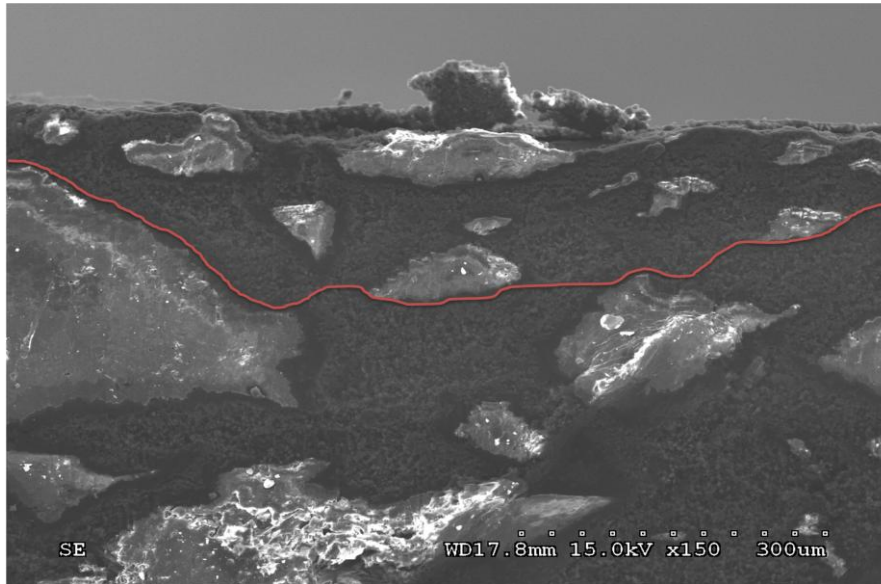


Figure 5-41: The SEM micrograph showing the formation of a softened area at a 20mm radius.

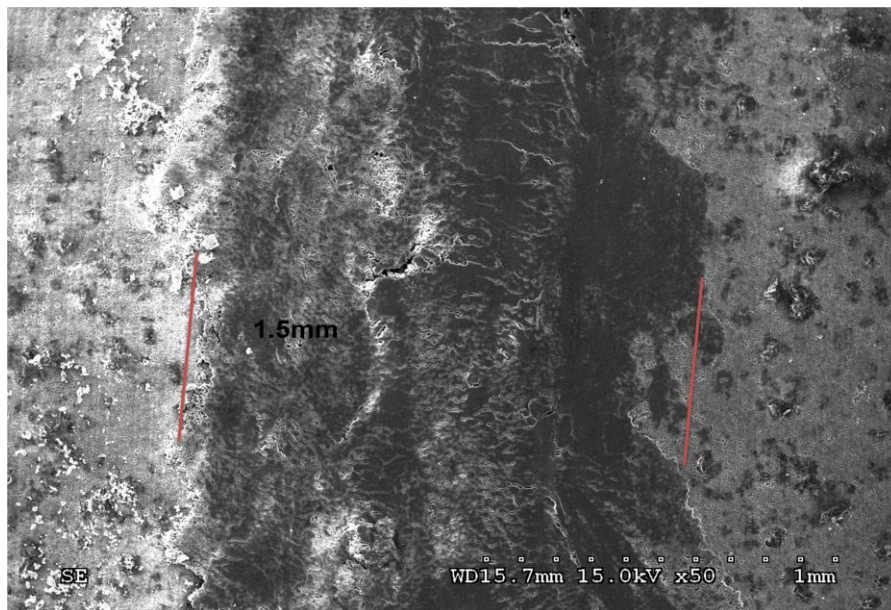


Figure 5-42: The diameter of the wear track made by the pin.

Figure 5-43, Figure 5-44, and Figure 5-45 show the measured coefficient of friction during each tribological test. Figure 5-44 shows the coefficient of friction that was obtained using a 2N load; which is the lowest coefficient of friction measured. The sample is predominantly erucamide and the test did not run for an extended amount of laps; therefore, during the experiment the pin did not have much contact with silica. Figure 5-43 and Figure 5-45 represent the coefficient of friction obtained using the same load but varied lap amounts. Both experiments show a similar coefficient of friction; however, since Figure 5-45 shows a greater amount of laps accounted for it is closer to the actual coefficient of friction for this particular weight percent of erucamide.

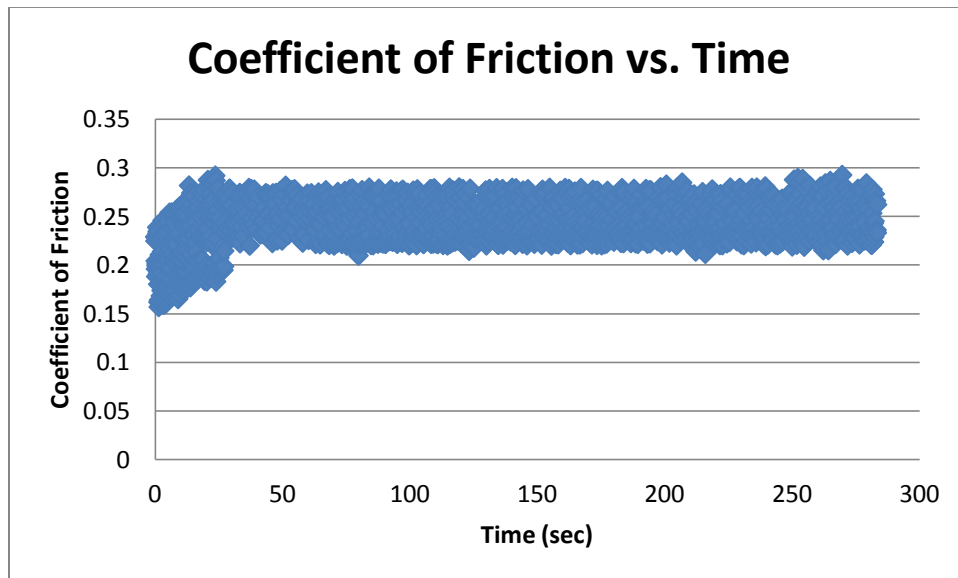


Figure 5-43: The coefficient of friction for the 15mm radius.

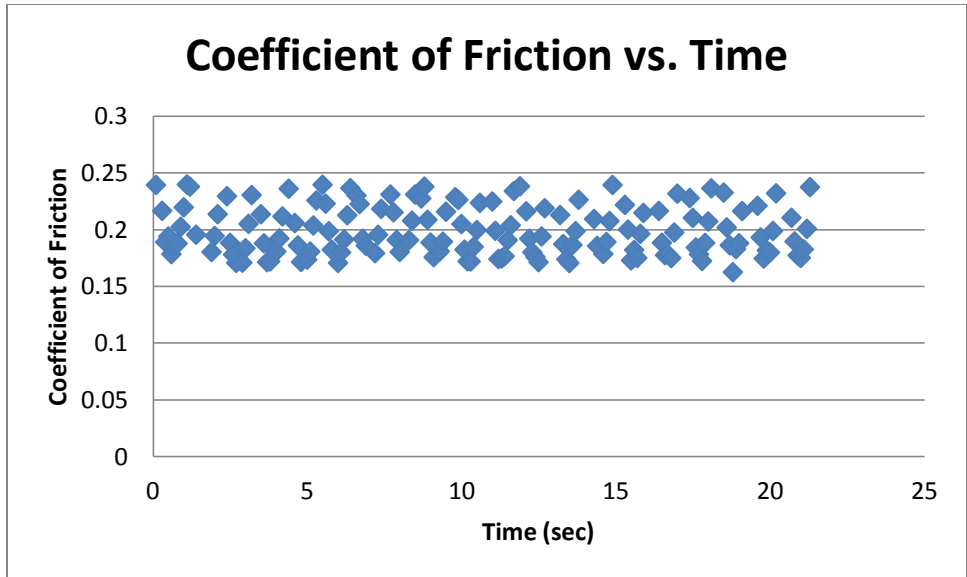


Figure 5-44: The coefficient of friction for the 17mm radius.

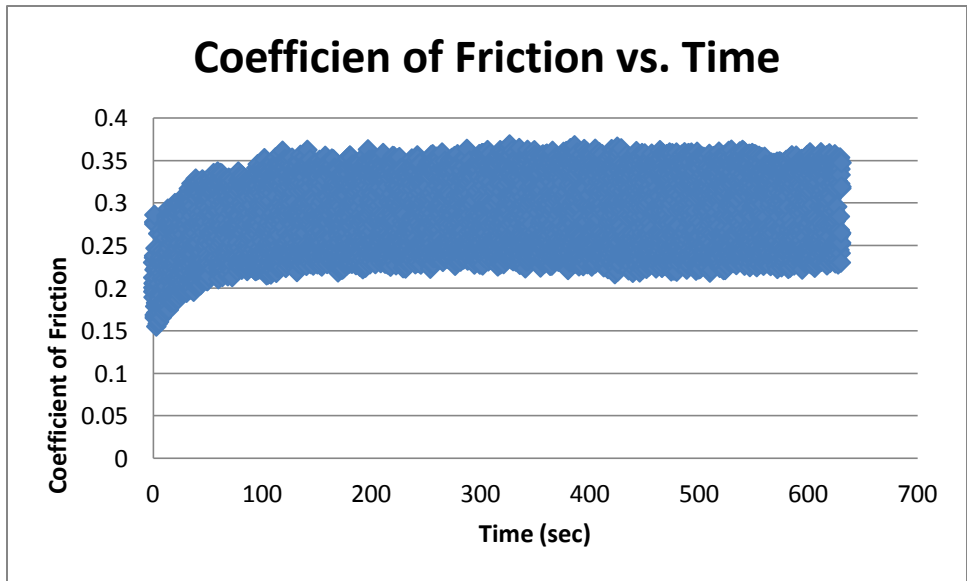


Figure 5-45: The coefficient of friction for the 20mm radius.

Figure 5-46, Figure 5-47, and Figure 5-48 show the relationship that temperature has with depth during sample 3's frictional heating experiments. During each experiment, a critical depth was achieved which is highlighted on each graph with a dashed line. This

critical depth corresponds to a critical temperature at which this depth will be achieved. Each figure has differing critical depths that were achieved; however, the critical temperature needed to achieve these depths is the same for all three experiments. This is due to the experiments having a very similar radius allowing for the cooling time to be the same.

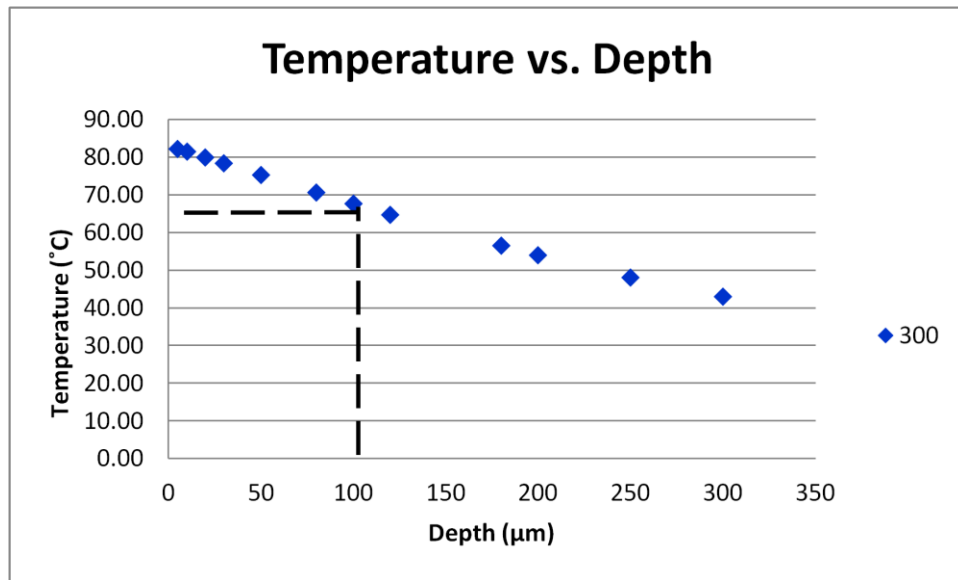


Figure 5-46: The relationship between temperature and depth for 15mm radius.

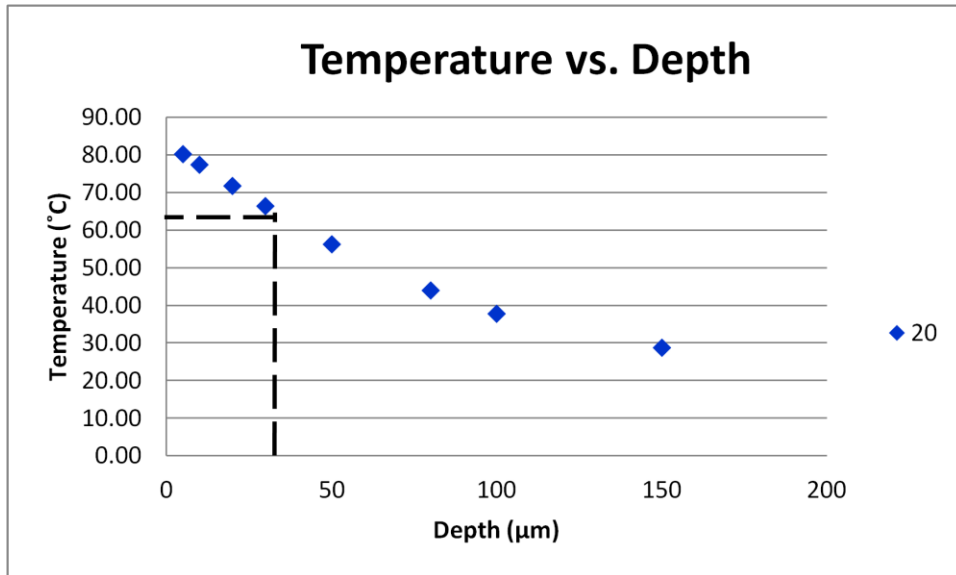


Figure 5-47: The relationship between temperature and depth for 17mm radius.

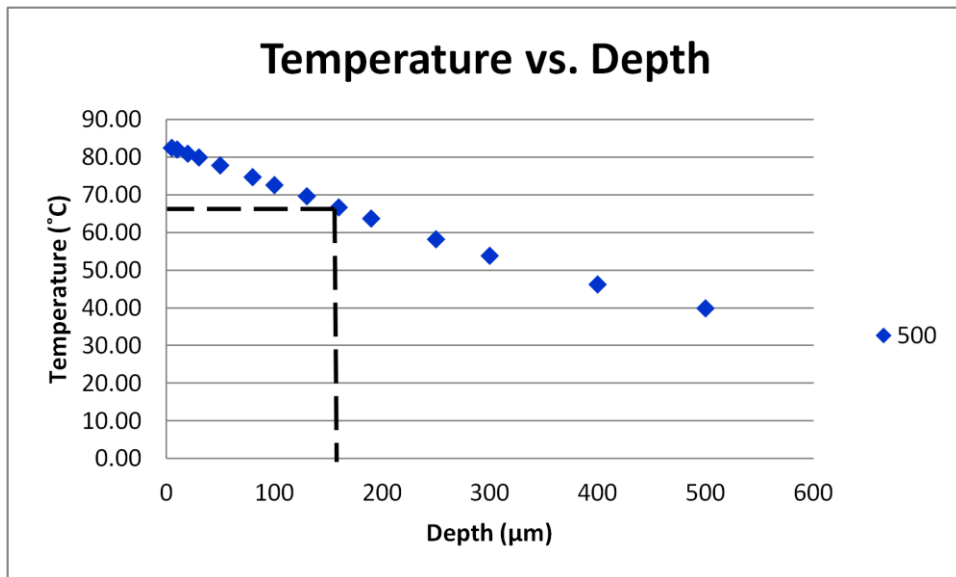


Figure 5-48: The relationship between temperature and depth for 20mm radius.

5.3.1.4 Total Frictional Work (\dot{W}_{Tf})

After completing the analysis on each sample's wear track, understanding the total frictional work that each load and amount of laps did was important. The utilization of

equation 4 and 5 provided the pressures from each experiment. These pressures as well as the known values of velocity and coefficient of friction were used in equation 2 to determine the frictional work produced per lap. Equation 6 was then used to determine the total frictional work produced by every lap. Table 5-9 shows the overall total frictional work that was done on each wear track.

Table 5-9: The total frictional work each sample experienced.

Sample:	Radius (mm):	Load (N):	Diameter (mm):	Area (m ²):	Pressure (N/m ²):	Coefficient of Friction (μ):	Velocity (m/sec):	Frictional Work- \dot{W}_f (J/sec/m ²):	Laps:	Total Frictional Work- \dot{W}_{Tf} (J/sec/m ²):	Depth (μm):
1	8	2	1.8	2.83×10^{-6}	7.07×10^5	0.53	0.1	3.75×10^4	200	7.50×10^6	260
1	11	2	1.5	2.36×10^{-6}	8.49×10^5	0.50	0.1	4.24×10^4	100	4.24×10^6	41
1	19	1	1.5	2.36×10^{-6}	4.24×10^5	0.56	0.1	2.38×10^4	250	5.94×10^6	88
2	10	2	1.7	2.67×10^{-6}	7.49×10^5	0.45	0.1	3.37×10^4	50	1.69×10^6	81
2	15	1	1.4	2.20×10^{-6}	4.55×10^5	0.62	0.1	2.82×10^4	20	5.64×10^5	27
2	20	2	1.8	2.83×10^{-6}	7.07×10^5	0.53	0.1	3.75×10^4	24	9.00×10^5	54
3	15	1	1.3	1.33×10^{-6}	7.53×10^5	0.25	0.1	1.88×10^4	300	5.65×10^6	111
3	17	2	1.0	7.85×10^{-7}	2.55×10^6	0.20	0.1	5.09×10^4	20	1.02×10^6	36
3	20	1	1.5	1.77×10^{-6}	5.66×10^5	0.26	0.1	1.47×10^4	500	7.36×10^6	177

Figure 5-49, Figure 5-50, and Figure 5-51 show the linear relationship between total frictional work and the depth acquired during each tribological experiment. When the sample requires more total frictional work to be done a higher thermal depth is achieved.

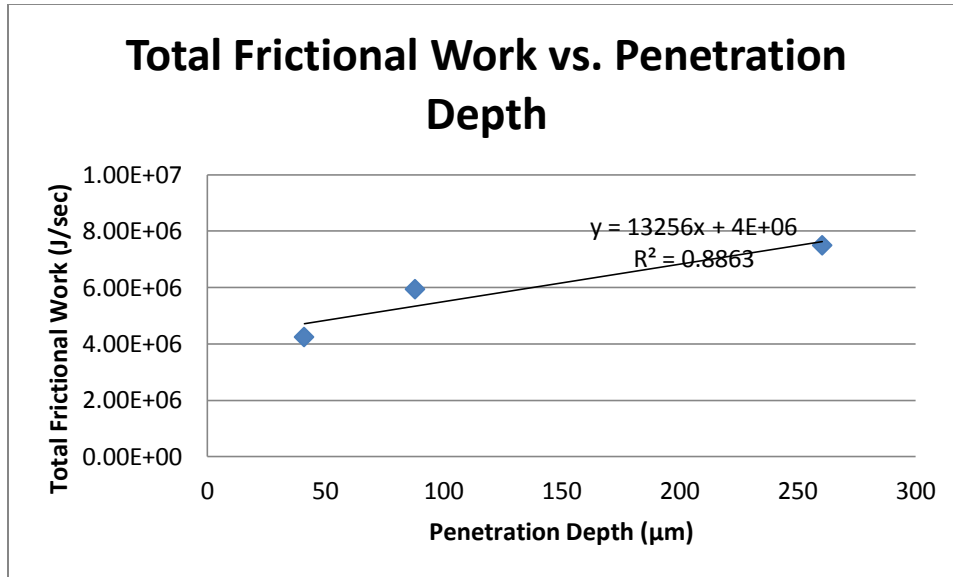


Figure 5-49: The relationship between total frictional work and depth for sample 1.

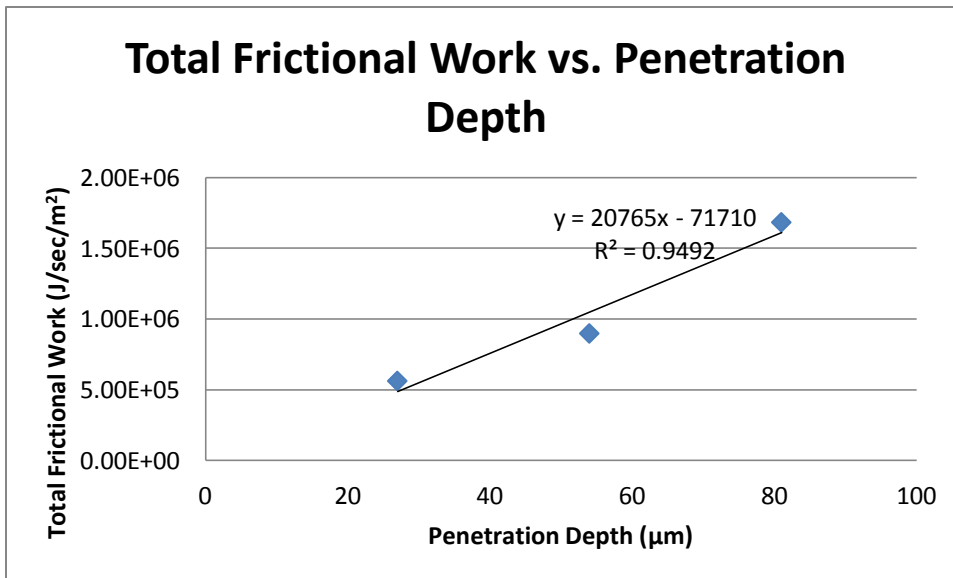


Figure 5-50: The relationship between total frictional work and depth for sample 2.

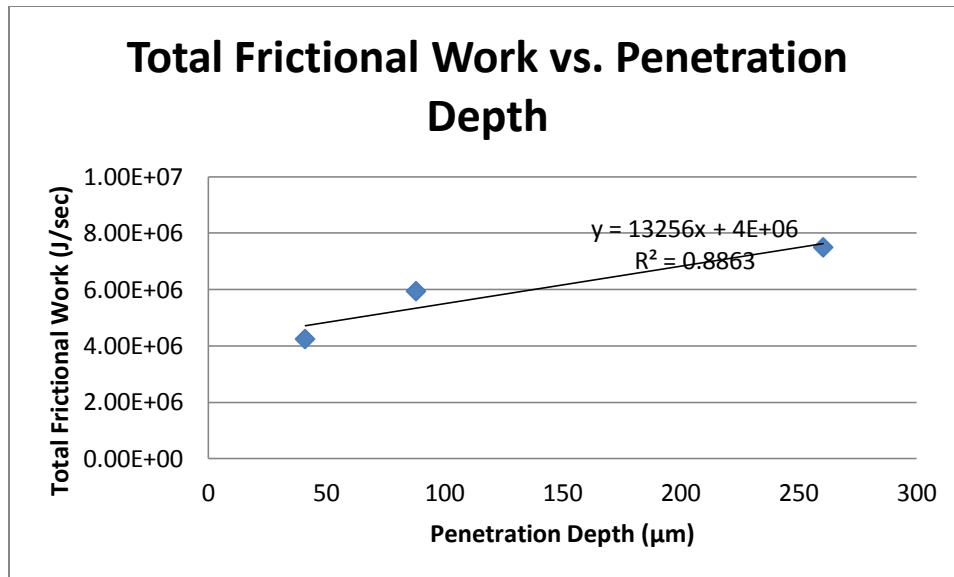


Figure 5-51: The relationship between total frictional work and depth for sample 3.

5.4 Discussion

During pelletization, a continual heat increase occurs which raises the internal temperature of the die's press channel. This temperature will induce a heat transfer to occur as the compacted material moves through the press channel. A melted shell layer then forms which causes a stable pellet to be extruded as shown in Figure 5-52.

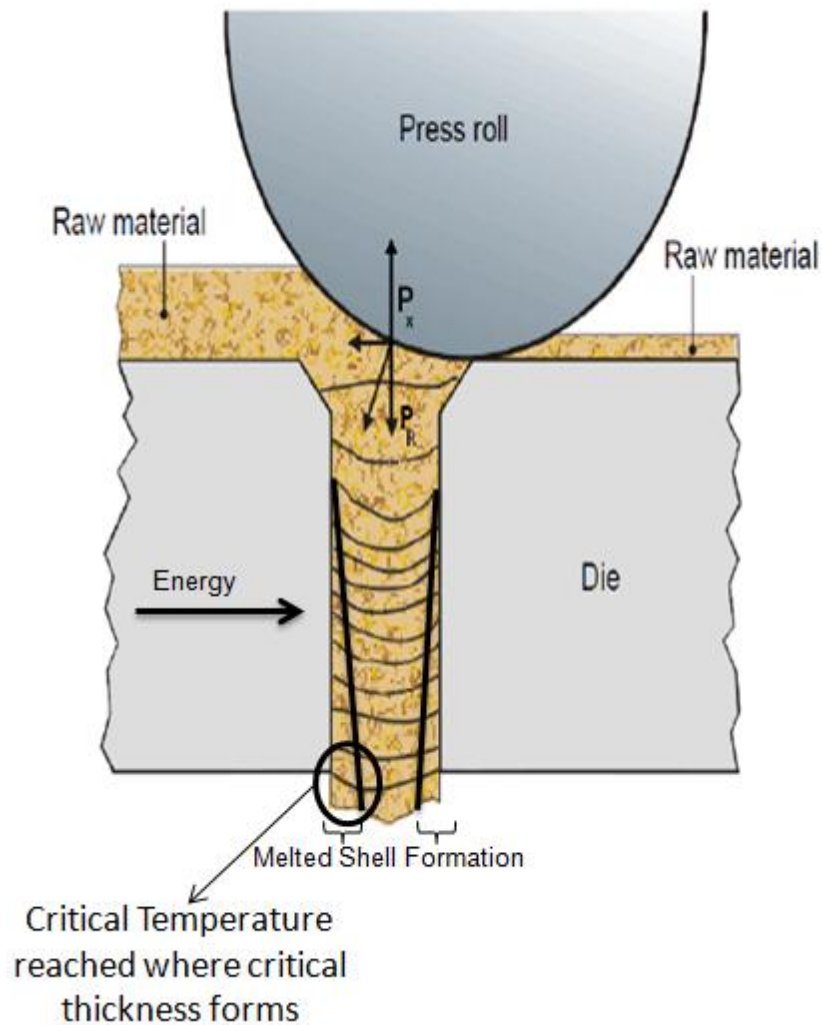


Figure 5-52: How the melted shell forms from the heat transfer that occurs inside the press channel (1).

The weight percent of erucamide had a positive effect on the thermal conductivity of the sample as seen in Figure 5-5. During characterization, a melted layer was seen which is similar to what occurs inside the die's press channel. Therefore, the relationship between the thermal conductivity and the penetration depth is shown in Figure 5-53.

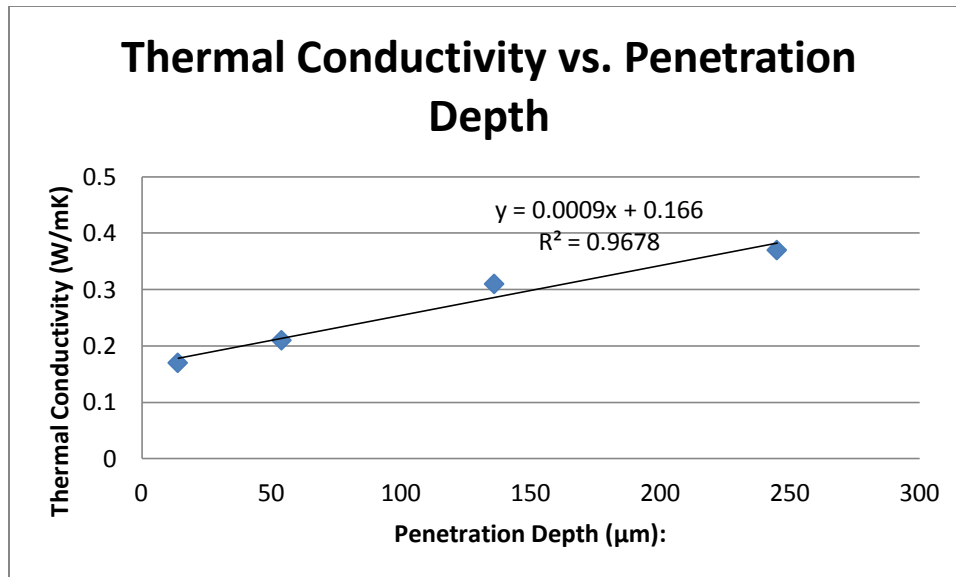


Figure 5-53: The relationship between thermal conductivity and penetration depth.

Figure 5-54, Figure 5-55, and Figure 5-56 show the relationship between the temperature and depth profile that each compacted pellet has. As the die reaches the melting temperature of the binder material, erucamide, a critical temperature is reached where a softened layer, known as the critical depth, begins to form providing stability to the pellet. As the amount of erucamide in each sample increases: a lower temperature to induce softening is seen, a lower critical temperature is seen, and a larger critical depth is formed.

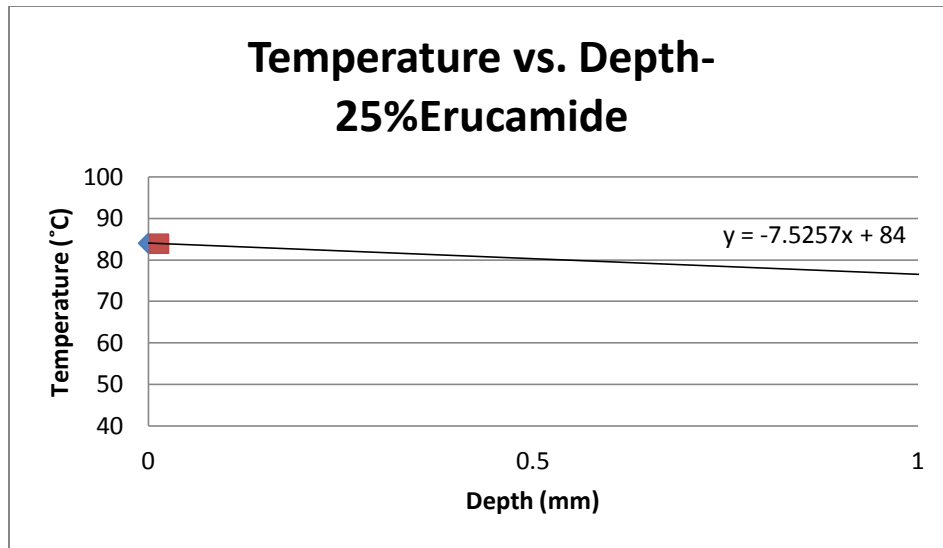


Figure 5-54: The relationship between temperature and depth for sample 1.

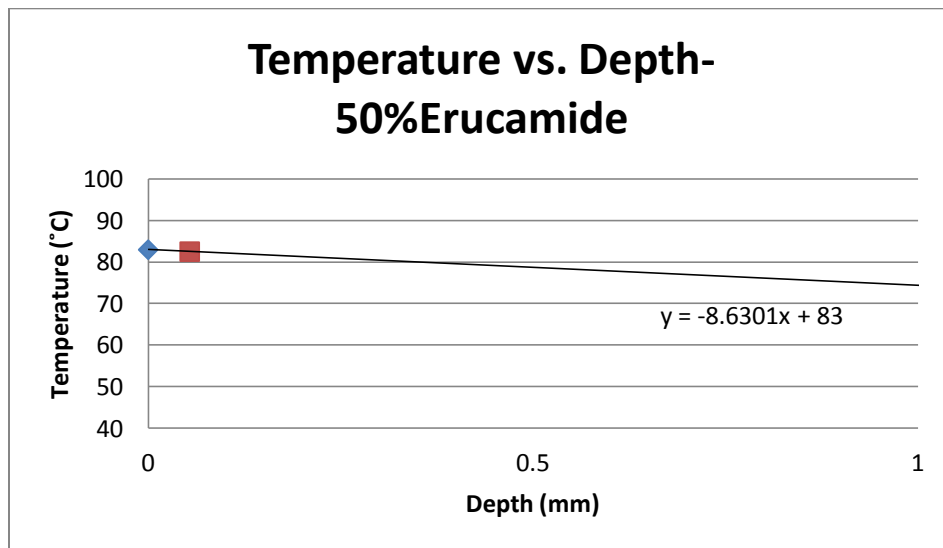


Figure 5-55: The relationship between temperature and depth for sample 2.

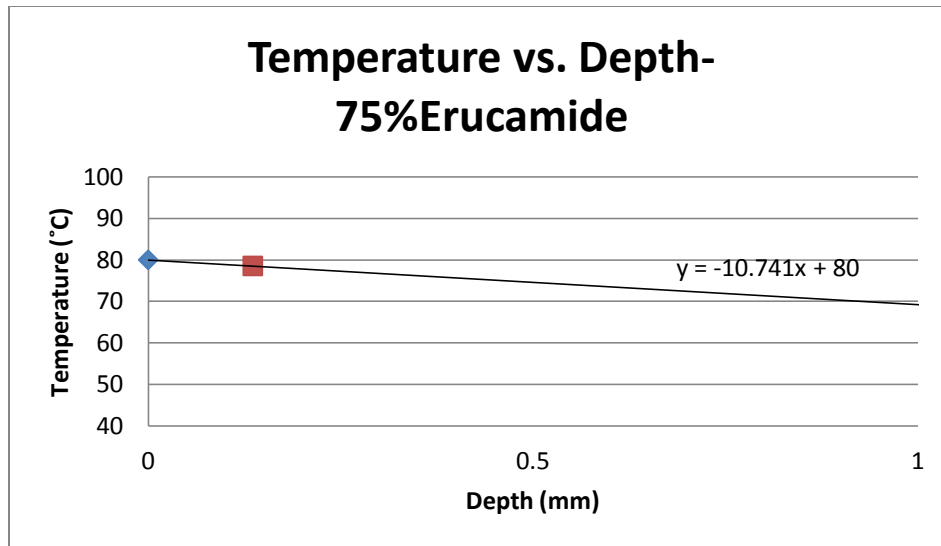


Figure 5-56: The relationship between temperature and depth for sample 3.

The weight percent of erucamide's effect of the frictional work is seen in Figure 5-57. The linear relationship that these two parameters form is negative. As the weight percent of erucamide increases, the coefficient of friction decreases. Therefore, the time that the pellet is inside the die's press channel decreases as well as the amount of heat that is able to penetrate into the pellet.

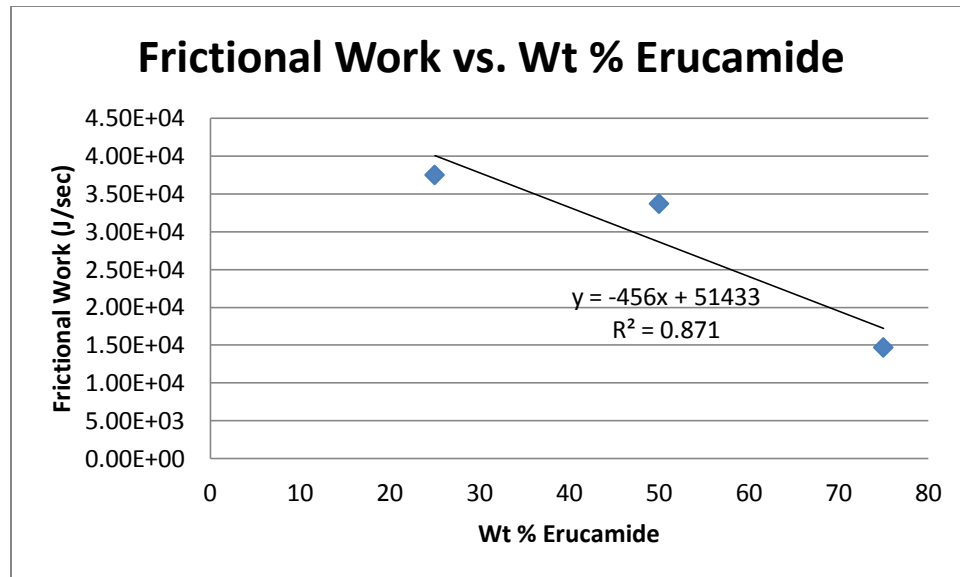


Figure 5-57: The change in frictional work as the wt% of erucamide increases.

During characterization, a melted layer was seen which is similar to what occurs inside the die's press channel. Total frictional work produces heat in the system which produces the softened shell layer thickness. Figure 5-58 shows how normalized total frictional work with thermal conductivity creates a penetration depth that can provide stability.

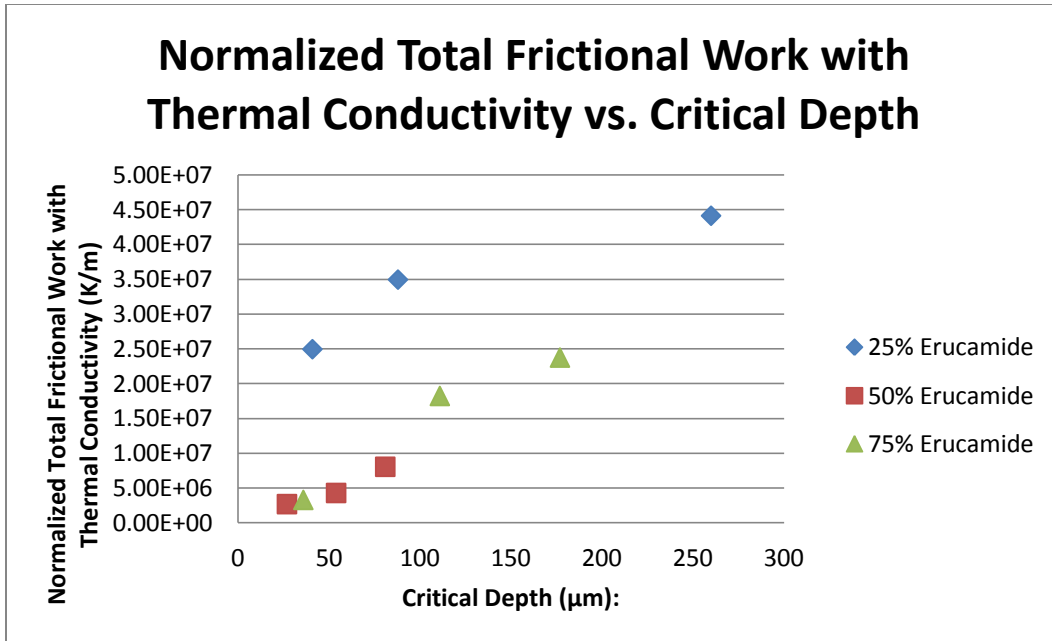


Figure 5-58: The relationship between normalized total frictional work with thermal conductivity and critical depth.

The samples with the greater weight percent of erucamide show how less heat needs to be generated in order to obtain the critical depth. Samples with less erucamide need to have a greater amount of heat in order to obtain the same critical depth. The material with 50% erucamide and 75% erucamide line up on the graph; therefore, the approximation can be related to the determination of critical depth that can provide stability.

Chapter 6

Conclusion

The thermal conductivity and frictional work for compacted additive blends with differing weight percents of erucamide and silica were found. These values were then compared to known values of paraffin wax and pure, precipitated silica in order to determine how each material affected the experimentally obtained result.

Samples with a higher weight percent of erucamide exhibited a larger heat transfer than samples made predominately of silica. With a stronger ability to provide heat transfer, erucamide's experimentally calculated thermal conductivity was higher than that of silica's.

The comparison between erucamide and paraffin wax showed that erucamide has a slightly higher thermal conductivity. The experimentally obtained thermal conductivity of silica was also higher than the known value. This occurrence is due to many different forms of precipitated silica that are readily available.

During times when friction arises, slip additives are expected to lower the coefficient of friction. The experimentally obtained coefficient of friction for erucamide shows that in the presence of a low weight percent of silica adequate slip is still present. The comparison between the known value and the experimentally obtained value shows that the value obtained is slightly higher. This is due to the presence of silica that is seen in the sample.

The dependence of thickness to form a stable pellet relies on the thermal conductivity of the materials used and the frictional work that goes into the system. When the thermal conductivity and frictional work are optimized the most accurate pellet thickness will be formed.

Appendix A

Determination of Critical Temperature

In order to establish a temperature profile to determine the critical temperature, T_x , from the critical depth found during the frictional heating experiments found on pages 65,66,73,74,80, and 81; a temperature gradient equation utilized for semi-infinite solids:

$$\frac{T_x - T_o}{T_s - T_o} = 1 - \operatorname{erf} \frac{x}{\sqrt{4 \times \alpha \times \tau}} \quad (9)$$

where T_o is room temperature at 25°C, T_s is the melting temperature of erucamide 83°C, α is the diffusivity of the material, τ is the residence time, and x is the penetration into the pellet (12).

The determination of diffusivity is by

$$\alpha = \frac{k}{\rho \times C_p} \quad (10)$$

where k is thermal conductivity of the sample, ρ is the density of the sample, and C_p is the heat capacity of the sample. The determination of residence time is by

$$\tau = \frac{2 \times \pi \times r}{v} \times L \quad (11)$$

where r is the radius, v is the velocity, and L is the number of laps.

References

1. *Recent Developments in Biomass Pelletization--A Review*. **Stelte, Wolfgang, et al.** 3, 2012, Vol. 7.
2. *Advancements in Additive Blends Technology for Polymers*. **Chatterjee, Ananda M, et al.** Houston : s.n., 2010. SPE Polyolefins 2010 International Conference.
3. **Zweifel, Hans, Maier, Ralph D and Schiller, Michael.** *Plastics Additives Handbook*. Munich : Carl Hanser Verlag, 2009. pp. 11, 45, 630-631, 660, 927-939. Vol. 6.
4. Anitblock-"The Basics". *Ampacet*. [Online] [Cited: 10 28, 2013.] <http://www.ampacet.com/usersimage/File/tutorials/antiblocks.pdf>.
5. **Croda.** *Crodamide Slip & Anti-block for easier processing & handling of polyolefins*. s.l. : Croda Polymer Additives.
6. *Importance of Temperature, Moisture Content, and Species for the Conversion Process of Wood Residues into Fuel Pellets*. **Nielsen, Niels Peter K, et al.** 2009, Wood and Fiber Science, pp. 414-425.
7. **Pietsch, Wolfgang.** *Agglomeration Processes*. Weinheim : Wiley, 2002. 3-527-30369-3.
8. *Thermal Conductivity of Packed Metal Powders*. **Hadley, G R.** 1986, International Journal Heat Mass Transfer, pp. 909-920.
9. *Standard Test Method for Thermal Conductivity of Solids by Means of the Guarded-Comparative-Longitudinal Heat Flow Technique*. **ASTM International.** West Conshohocken : ASTM International, 2009. E 1225-09.
10. *Analytical Modeling and Characterization of Heat Transfer in Thermally Conductive Polymer Composites Filled with Spherical Particulates*. **Leung, Siu N, et al.** 2012, Composites: Part B.
11. *Friction Science and Technology: From Concepts to Applications*. s.l. : Taylor & Francis Group, LLC, 2009. pp. 171-177.
12. **Tadmor, Zehev and Gogos, Costas G.** *Principles of Polymer Processing*. 2. s.l. : John Wiley & Sons, Inc., 2006. pp. 178-227.
13. **Wypych, George.** *Handbook of Antiblocking, Release, and Slip Additives*. Toronto : ChemTec Publishing, 2005.
14. *Experimental and analytical thermal study of PTFE composite sliding against high carbon steel as a function of the surface roughness, sliding velocity and applied load*. **Tzanakis, I, et al.** 1-2, s.l. : Elsevier, 2013, Vol. 303.
15. *Frictional Behaviour of CaCo3 Powder Compacts*. **Berg, Sven, et al.** 228, s.l. : Elsevier B.V., 2012, Powder Technology, pp. 429-434.

16. *Thermal Conductivity of Metal Powder-Polymer Feedstock for Powder Injection Moulding*. **Kowalski, L, Duszczuk, J and Katgerman, L.** 1999, Journal of Materials Science, pp. 1-5.
17. *Thermophysical Comparison of Five Commercial Paraffin Waxes as Latent Heat Storage Materials*. **Ukrainczyk, N, Kurajica, S and Sipusic, J.** 2, Zagreb : Chemical & Biochemical Engineering Quarterly, 2010, Vol. 24.
18. **Graves, Ronald and Zarr, Robert.** *Insulation Materials: Testing and Applications*. West Conshohocken : American Society for Testing and Materials, 1997.
19. *Dynamic Mechanical Analysis and Tribological Properties of NR Vulcanizates with Fly Ash/Precipitated Silica Hybrid Filler* . **Thongsang, Sirinthorn, et al.** 53, s.l. : Tribology International, 2012.
20. **Maltby, A.J. and Read, M.** *Effect of Temperature on the Slip and Blocking of Polyolefins Containing Various Fatty Acid Amides*.
21. *AFM Characterization of Surface Segregated Erucamide and Behenamide in Linear Low Density Polyethylene Film*. **Ramirez, Maria, Hirt, Douglas and Wright, Laura.** 1, s.l. : Nano Letters, 2002, Vol. 2.
22. Glycerol Monostearate. [Online] 20. [Cited: 10 24, 2012.] http://sci-toys.com/ingredients/glycerol_monostearate.html.
23. **Callister Jr., William D and Rethwisch, David G.** *Materials Science and Engineering an Introduction*. s.l. : John Wiley & Sons, Inc., 2010. pp. 160, 782, 789. Vol. 8.
24. *Determination of Effective Thermal Conductivity and Specific Heat Capacity of Wood Pellets*. **Guo, Wendi, et al.** s.l. : Elsevier Ltd., 2012, Fuel.
25. **Allcock, Harry R.** *Introduction to Materials Chemistry*. Hoboken : John Wiley & Sons, Inc., 2008. pp. 70-71.
26. *Toward an Understanding of Controlling Parameters in Softwood and Hardwood Pellets Production*. **Holm, Jens, et al.** 6, s.l. : Energy & Fuels, 2006, Vol. 20.

Biographical Information

During her academic career, she received a Bachelor's of Science Cum Laude in Biochemistry from Texas Woman's University in 2011. She participated in academic organizations Kappa Epsilon Mu and the National Society of Leadership and Success. After leaving TWU, she joined the SaNEL group run by Dr. Meletis at UTA in 2012. Here she studied the affect that thermal conductivity and frictional heat had on polymer additives. Her future plans include working at a company that utilizes different characterization techniques and biomaterials.